Soil Dynamics and Earthquake Engineering 82 (2016) 170–195

Contents lists available at ScienceDirect

Soil Dynamics and Earthquake Engineering

journal homepage: www.elsevier.com/locate/soildyn

A stochastic ground motion accelerogram model for Northwest Europe

Carlos Medel-Vera *, Tianjian Ji [1]

School of Mechanical, Aerospace and Civil Engineering, Pariser Building, Sackville Street, The University of Manchester, Manchester M13 9PL, UK

ARTICLE INFO

Article history:
Received 1 September 2015
Received in revised form
22 October 2015
Accepted 17 December 2015
Available online 8 January 2016

Keywords:
Accelerograms
Stochastic models
Synthetic records
Earthquake ground motions
Northwest Europe
United Kingdom

ABSTRACT

This article presents a stochastic ground-motion accelerogram model for Northwest Europe which simulates accelerograms compatible with seismic scenarios defined by earthquake magnitudes $4 < M_w < 6.5$, distance-to-site 10 km $< R_{epi} <$ 100 km and different types of soil (rock, stiff and soft soil). This model is developed based on Rezaeian and Der Kiureghian (2008, 2010) [1,2] and is a set of predictive equations that define a time-modulated filtered white-noise process. Such predictive equations were calibrated by means of the random-effects regression technique using a subset of the European database of accelerograms. The model is validated in terms of PGA, PGV and spectral accelerations using GMPEs for the UK, Europe and Middle East, and other Stable Continental Regions. This model is the first of its kind for NW Europe.

1. Introduction

In order to conduct seismic probabilistic risk analysis (SPRA), it is necessary to perform non-linear time history (NLTH) analysis of a structural model. Ultimately, this will lead to an estimation of the probability of unacceptable performance of the structure for the defined seismic hazard [3–5]. The main obstacle for conducting NLTH analysis of structures is the scarcity of accelerograms able to realistically represent the frequency content, intensity distribution and the strong shaking phase duration of recordings compatible with the scenarios that contribute most strongly to the hazard of the site selected [2]. This is an even more remarkable problem for areas of medium-to-low seismicity because: (i) strong earthquakes rarely occur, and (ii) those areas have limited monitoring networks [6]. For the United Kingdom (UK), which is a zone of relatively low seismicity, seismic hazard cannot be disregarded as strong earthquakes can still occur and may jeopardise the structural integrity of high-risk structures [7]. The paucity of accelerograms has led structural engineers to using techniques based on selecting, scaling and matching procedures applied to available records [8–10]. Even though the legitimacy and applicability of these procedures have been the subject of ample discussion in the literature [11–13], they are widely accepted and used by researchers and practitioners [14–16]. In general, these procedures are intended to match a spectral shape predicted by ad-hoc ground motion prediction equations (GMPEs). Currently, GMPEs play a critical role in seismic hazard and risk analysis and much research effort has been placed on the development of such models. Examples of state-of-the-art GMPEs are: the NGA-West2 Research Project [17], a major long-term project that developed attenuation models for active tectonic regions; and similarly for Europe and the Middle East, a new generation of GMPEs developed using the most recent pan-European strong-motion databank [18]. However, as SPRA requires the direct specification of sets of accelerograms, the use of GMPEs is actually an unnecessary intermediate step towards this objective [19]. Promising trends in earthquake engineering have been developed aiming at the replacement of GMPEs in seismic hazard and risk analysis for more rational approaches [20–22], as the one proposed in this work.

Stochastic generation of artificial accelerograms can be used to overcome the scarcity of ground-motion records. Currently, there are three techniques used to generate artificial accelerograms [23]: (i) mathematical or source-based models based on physical/seismological principles (e.g. Halldórsson et al. [24]; Liu et al. [25]); (ii) experimental or site-based models using measured/experimental data (e.g. Mobarakeh et al. [26]; Rofooei et al. [27]; Sgobba et al. [28]); and (iii) hybrid models that combine both approaches (e.g. Graves and Pitarka [29]). As pointed out by Boore [30], source-based models are mostly developed by seismologists in an attempt to explain the physics behind earthquake generation (e.g. source mechanism and propagation path). On the other hand, experimental models are mainly developed by engineers to obtain accelerograms using fitting techniques. From a structural engineering point of view, the main setback in using source-based

E-mail addresses: carlos.medelvera@postgrad.manchester.ac.uk (C. Medel-Vera), tianjian.ji@manchester.ac.uk (T. Ji).
* Corresponding author. Tel.: +44 161 306 2361; fax: +44 161 306 4646.
[1] Tel.: +44 161 306 4604; fax: +44 161 306 4646.

http://dx.doi.org/10.1016/j.soildyn.2015.12.012
0267-7261/

models is that a profound knowledge of the governing seismological features of the site of interest is needed.

For the UK, the underlying tectonic mechanism that causes earthquakes is not yet fully understood [31] and there is little correlation between the pattern of earthquake occurrence and the structural geology of Britain [32]. Additionally, the database of British earthquakes is mainly composed of accelerograms recorded from small magnitude earthquakes, M_w 2–4.5 [33]. Consequently, the nature of accelerograms (in terms of intensity, frequency content and time duration) is still unknown for stronger earthquakes, say M_w 6, that may occur in the UK [34]. This situation is critical for the British nuclear industry, as such a magnitude is in the order of earthquakes that need to be included in seismic risk analyses, when considering a design basis event of 10,000 years return period [35]. In order to help fill this gap, a site-based model based on Rezaiean and Der Kiureghian [1,2] is proposed that stochastically simulates two-component horizontal accelerograms compatible with any seismic scenario defined by an earthquake of magnitude $4 < M_w < 6.5$, distance-to-site $10 < R_{epi} < 100$ km and different types of soil (rock, stiff and soft soil). These accelerograms can be used to perform SPRA on high-risk structures in the UK and NW Europe. The model is based on a set of predictive equations for parameters that govern a fully non-stationary stochastic process that is used to simulate earthquake accelerograms. The predictive equations are calibrated using regression analysis on a dataset of accelerograms recorded in the tectonic region to which the UK belongs. The simulation of accelerograms is entirely made in the time domain, it essentially involves the generation of random variables and uses a few input data readily available in structural engineering practice. This model is the first of its kind for the general region of NW Europe including the UK. The model is validated through a comparison of estimated peak ground accelerations (PGA), peak ground velocity (PGV) and spectral accelerations with those produced by GMPEs for similar target geographical regions.

This article is organised as follows: Section 2 gives a full description of the target geographical region of interest and defines the dataset of accelerograms selected for this work. The explanatory variables selected to perform regression analyses for the predictive equations are also discussed in this section. Section 3 provides the stochastic process to simulate accelerograms and gives an example of simulation using a single record from NW Europe as the target accelerogram. This section also reports predictive equations for the parameters that govern the stochastic process and their regression coefficients, as a function of earthquake magnitude, distance-to-site and type of soil. Section 4 provides the procedure to simulate accelerograms and validates such simulations against recorded accelerograms from NW Europe and GMPEs. Such attenuation models are from three main regions: the UK, Europe and the Middle East, and other Stable Continental Regions (SCRs) whose tectonic behaviour is expected to be similar to NW Europe's. Section 5 discusses further aspects regarding the calibration and use of the model proposed, its validity, its limitations and its constraints imposed by traditional attenuation relations. Finally, the conclusions from this work are summarised in Section 6.

2. Target geographical region and model parameters

The United Kingdom (UK) is considered to be an intraplate region with moderate-to-low seismicity levels [32]. In seismological terms, it is part of one of several Stable Continental Regions (SCRs), possessing unique tectonic features. These features are mostly linked to the timing and nature of crustal deformation. Johnston et al. [36] reported a comprehensive study on the tectonic character and seismicity of SCRs worldwide. They defined nine major and some minor SCRs that cover approximately 2/3 of all continental crust (and 1/4 of all crust: continental, oceanic and transitional); however, they are only responsible for 0.22% of the global seismic moment release rate. This reflects the relatively low seismicity levels in SCRs (such as the UK) compared to tectonically active zones (such as California and Japan). In spite of this fact, seismic hazard in the UK is non-negligible, as strong ground motions capable of compromising the structural integrity of strategic facilities can still occur [7]. In terms of magnitudes, two of the most significant known earthquakes which occurred in the UK were in 1382 and 1580 in the Dover Straits area. Both events were of magnitude approximately M_L 5.75 [32]. This magnitude is close to the largest known earthquake occurred in the UK: an event M_w 5.8 occurred in the English Caledonides region of the North Sea in 1931 [37]. Additionally, in a study by Musson [38], it was suggested that a major earthquake M_w 7 could have occurred offshore in recent geological times in the NW European passive margin near Britain. Examples of the latest moderate earthquakes which have occurred in the UK are: (i) a M_L 4.7 event in September 2002 in Dudley, West Midlands [39] (ii) a M_w 4 event in April 2007 in Folkestone, Kent [40], and (iii) a M_L 5.2 event in February 2008 near Market Rasen, Lincolnshire [41]. The current state-of-the-art knowledge on the seismicity and seismic hazard zoning of the UK is reported in Musson and Sargeant [42].

Several problems arise when developing predictive models in zones that are not tectonically active. The database of British earthquakes is mainly composed of accelerograms recorded from a few small magnitude earthquakes. The use of such information, in the prediction of accelerograms of moderate-to-strong earthquakes, can produce unreliable and unrealistic results [42]. It is also not entirely consistent to make predictions based on accelerograms recorded in different SCRs from the region of interest. Even though all SCRs share the same fundamental crustal features, there is no overall agreement whether such regions are similar in terms of their earthquake generation and attenuation mechanisms [34]. Therefore, the predictive model proposed in this work is based on the assumption that the nature of accelerograms (intensity, frequency content and time duration) of strong magnitude earthquakes in Britain would be similar to those strong earthquakes occurred in the same SCR to which the UK belongs, namely NW Europe. This assumption effectively avoids both the use of small-magnitude records to predict moderate-to-large accelerograms and the inclusion of earthquakes from other SCRs or other intraplate regions.

2.1. Definition of Northwest Europe

A systematic description of the boundaries of NW Europe was needed. Various definitions have been reported in the literature, for example, Goes et al. [43] defined it as a relatively small area excluding the UK and the Scandinavian peninsula, whereas Ambraseys [44] defined it as a more expanded area including the UK and most of Norway and Sweden. The approach used in this work to define boundaries for NW Europe, was the Flinn–Engdhal (F–E) regionalisation scheme [45], comprising the countries and areas indicated in Table 1 and shown in Fig. 1. Such a definition of NW Europe is within the limits of the European SCR defined by Johnston et al. [36]. Hence, it can be considered as a subset of the SCR of interest, possessing relatively uniform tectonic features.

Regarding the size of the dataset, it is acknowledged that current databases of accelerograms have experienced a particularly rapid expansion in recent years to reach several thousands of available earthquake recordings [17,46]. Such an expansion has led a fast development of GMPEs: Douglas [47] showed that more

Table 1
Countries/areas that comprise the NW Europe F–E region [45].

Eire	Belgium
United Kingdom	Denmark
North Sea	Germany
Southern Norway	Switzerland
Sweden	Northern Italy
Baltic Sea	Austria
France	Czech and Slovak Republics
Bay of Biscay	Poland
The Netherlands	Hungary

than 15 new of these models are published every year. These models normally combine seismic events from different regions in order to calibrate them using datasets composed of a few thousands of recordings. One advantage of using stochastic accelerogram models is that it is possible to obtain similar results as those predicted by GMPEs but using smaller datasets. For example, Rezaeian and Der Kiureghian [1] showed that using a small subset of 206 accelerograms of the NGA database, a particularly good agreement was obtained with four GMPEs of the NGA Project, which in turn were calibrated using a large number of recordings ranging from 1574 to 2754. In this light, a small dataset of

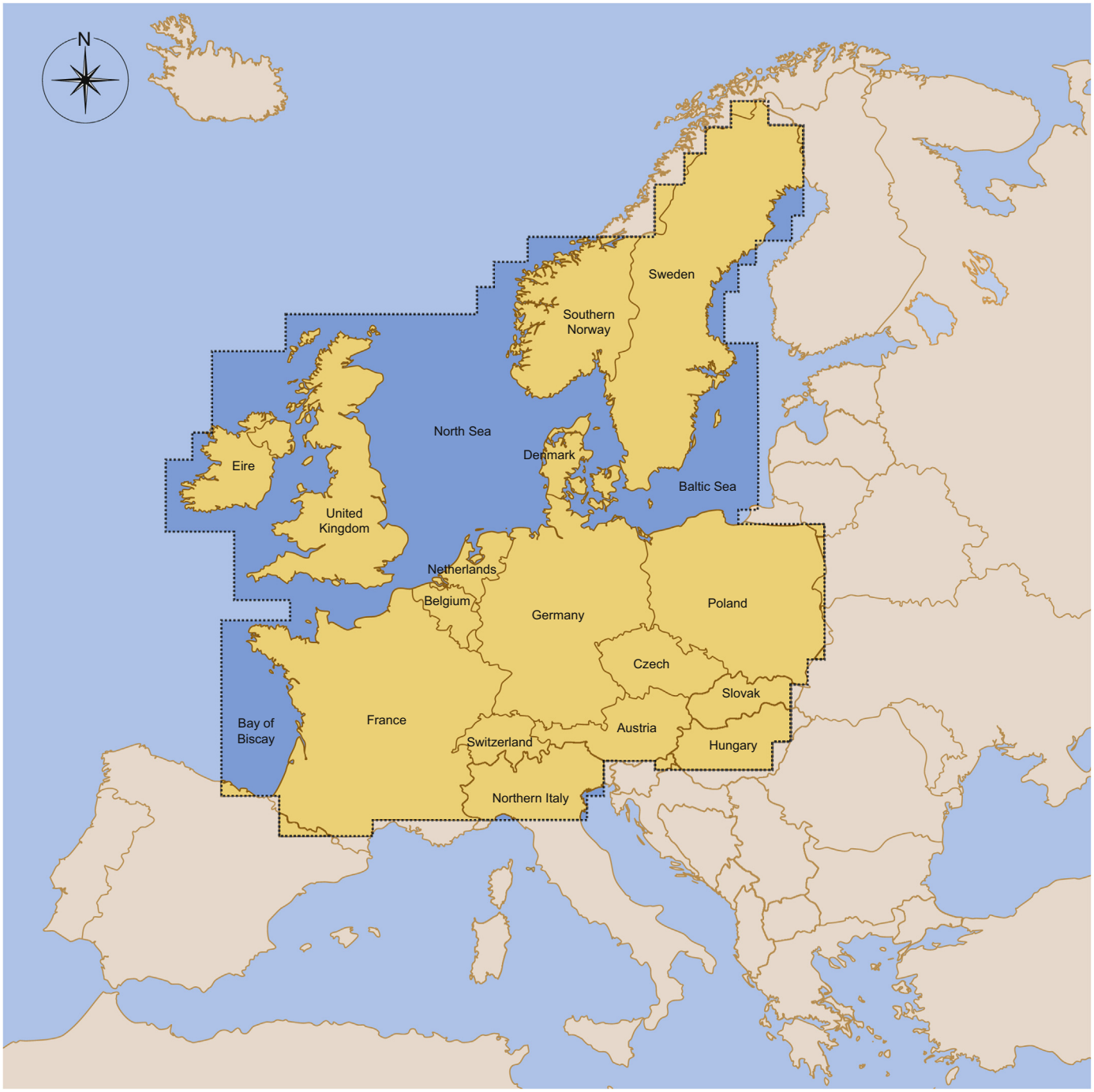

Fig. 1. Map of the NW Europe F–E region [45].

recordings from the European database was used in this work, yet a good agreement was expected to obtain with predictions made with European GMPEs.

A suitable pan-European on-line database in the public domain providing accelerograms from the countries/areas in Table 1, was the Internet Site for European Strong-Motion Data (ISESD) [33]. It is acknowledged that the existence of the most recent pan-European strong-motion databank [18] unifies all European databases of accelerograms. However, such a database was unavailable in the public domain at the time of writing. The variables considered for the model proposed in this work are: (i) earthquake magnitude, (ii) earthquake distance-to-site and (iii) type of soil. These variables are described in detail in the following sections. It is not possible to include the style of faulting in the present model, but a discussion on this topic is provided in Section 2.5.

2.2. Earthquake magnitude: scale and bounds

For this work, the moment magnitude scale (M_w) is used in calibrating the prediction model. Several earthquake magnitudes in the ISESD database are reported in different scales, namely, the surface-wave magnitude (M_s), the body-wave magnitude (m_b) and the local magnitude (M_L). Hence, their equivalent magnitudes in M_w need to be estimated. Conversion scale formulae, based on regression analysis, have been reported in literature [48]. However, the conversion formulae reported by Johnston [49] are used in this work as they were calibrated for SCRs only. Regardless of the conversion formulae used, it is acknowledged that their use can increase the uncertainty of the model [50]. Nevertheless, the use of conversion formulae is unavoidable when dealing with moderate-to-low seismic areas as the calculation of M_w for relatively small earthquakes is rarely undertaken.

For the lower bound magnitude in the dataset, M_w 4 was selected. This value is in line with lower bounds used for seismic hazard assessments in the UK [20]. It is acknowledged that some GMPEs intended for use in the UK [6,37] used a minimum magnitude of M_w 3. However, it is considered that such small earthquakes have little, or no, significance for structural engineering purposes. For the upper bound magnitude, M_w 6.5 was used. This magnitude has also been considered as the maximum value in seismic hazard assessments in Britain [42]. This value is also the maximum earthquake magnitude found in the ISESD database for the F–E region indicated in Table 1.

2.3. Earthquake distance: metric and bounds

Several distance metrics have been used in earthquake engineering: epicentral distance (R_{epi}), hypocentral distance (R_{hyp}), rupture distance (R_{rup}) and the Joyner–Boore distance (R_{JB}) [51]. R_{epi} and R_{hyp} are metrics that consider the earthquake rupture as a point source. These metrics are suitable for low-to-moderate magnitudes, but inappropriate for moderate-to-large earthquakes as the source comprises an extended area. In such scenarios, R_{rup} and R_{JB} are more appropriate. For the information source for this work, the ISESD database reports two distance metrics: R_{epi} and R_{JB}, although the latter is only reported for earthquake magnitudes greater than 6. As the completeness of R_{JB} is sparse, R_{epi} is used in this work. It is worth mentioning that R_{epi} and R_{JB} are closely related to each other, as both are defined along the surface of the Earth. The underlying assumption of using R_{epi} is that the variability of focal depths was not considered in the calibration of the prediction model proposed. British earthquakes, on average, can be considered to be shallow crustal. Small magnitude events have focal depths $\sim$10 km; for stronger events, the depth increases up to $\sim$25 km [52].

For this work, accelerograms recorded at R_{epi} less than 10 km were discarded. This is to exclude some intrinsic features of near-fault records that would need to be addressed in a separate model, e.g. severe directivity pulses [53], which can have a significant influence on the frequency content of accelerograms. The largest R_{epi} found in the ISESD database for the F–E region in Table 1 was 193 km. Certainly, the model proposed does not apply when dominant scenarios are controlled by near-fault conditions. However, some potential nuclear sites in the UK are controlled by seismic scenarios whose distances are $\geq$10 km [20,35,54], in which case the model proposed is fully applicable.

2.4. Type of soil

For the case of GMPEs calibrated for use in Western United States, the type of soil has been included quantitatively, through the average shear wave velocity in the upper 30 m (V_{S30}) [55]. However, for Europe and the Middle East, the type of soil was traditionally included qualitatively by directly specifying the class site (e.g. 'rock', 'stiff soil', etc.) (e.g [56,50]), although the most recent models have been calibrated by direct specification of V_{S30} [57]. For the specific case of UK models, the site classification has been considered qualitatively or it has not been included [37]. For NW Europe, the ISESD database reports both V_{S30} and types of soil based on the Boore et al. [58] criteria: very soft soil: $V_{S30} < 180$ m/s; soft soil: $180 < V_{S30} < 360$ m/s; stiff soil: $360 < V_{S30} < 750$ m/s; rock: $V_{S30} > 750$ m/s. For earthquakes from the F–E region in Table 1, the information for V_{S30} is not complete, but qualitative site classification is provided. Therefore, three types of soil are included: (i) rock, (ii) stiff soil and (iii) soft soil. Very soft soil is discarded as it is unlikely that any major civil structure would be built on such soil.

2.5. Faulting mechanism

For the case of GMPEs, the style of faulting is normally included qualitatively (e.g. 'strike-slip', 'normal', 'reverse') [17,57]. For the UK, the style of faulting is not normally included [37]. This is possibly due to the fact mentioned in Section 1 that the underlying tectonic mechanism causing earthquakes in the UK is not yet fully understood. Baptie [31] reported that the style of faulting related to British earthquakes is mostly strike-slip, but may be reverse and, at a lesser extent, normal. The ISESD database does report the style of faulting, but the information is not complete for the F–E region indicated in Table 1. Therefore, for this work, the faulting mechanism could not be included in the prediction model.

2.6. Summary of the dataset

Only accelerograms recorded in free-field conditions are included. All those recorded in buildings or other types of structure are discarded. Also, aftershocks are included in the dataset used in this work as the separation between mainshocks and aftershocks in European earthquakes has an unclear effect [59]. In summary, the dataset (last accessed 02.09.2013) considered for this work included free-field two-component horizontal accelerograms from earthquakes magnitude M_w 4–6.5, recorded at epicentral distances between 10 and 193 km, considering three generic types of soil: rock, stiff soil and soft soil. The total number of accelerograms obtained for the F–E region (Table 1) was 220 records (110 pairs of horizontal accelerograms) obtained from 43 earthquakes. In terms of the type of soil, the dataset used in this work includes 42 pairs of horizontal

accelerograms recorded in rock, 52 in stiff soil and 16 in soft soil. Fig. 2 provides a graphical summary of this dataset. Table 2 provides information of the earthquakes in this dataset.

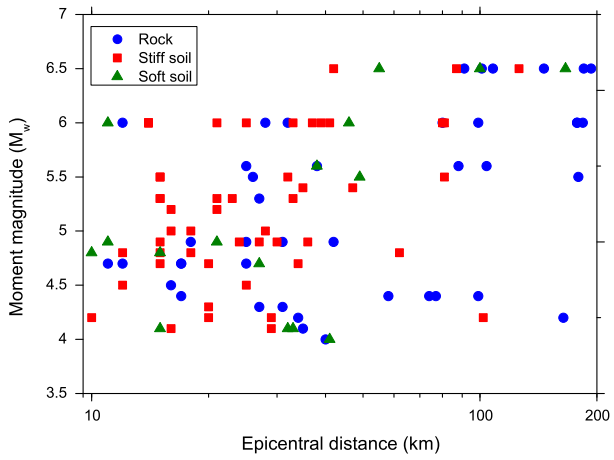

Fig. 2. Distribution of magnitudes and distances for the dataset used in this work.

3. Stochastic process and model calibration

As mentioned in Section 1, site-based or experimental models make simulations based on measured data of recorded earthquakes using mathematical fitting techniques. For the simulation of accelerograms, the majority of such models consist of the modulation in time of a filtered white-noise process. The key issue for these models is their ability to account for non-stationarity in the time and frequency domains. Examples of site-based models can be found in Mobarakeh et al. [26], Rofooei et al. [27], Sgobba et al. [28]. The work presented in this article has taken advantage of the stochastic process reported by Rezaeian and Der Kiureghian [2], as it presents particular features that ease its calibration and use for structural engineering purposes. The main features are: (i) temporal and spectral non-stationarities are totally decoupled; this eases the selection of functional parameters governing both non-stationarities to be fitted to real accelerograms, (ii) the model works exclusively in the time domain; hence Fourier analysis or other analyses in the frequency domain are not required, and (iii) the simulation of accelerograms essentially involves the generation of random variables, avoiding the use of more complex numerical analysis. In this section, the functional parameters of the stochastic process that characterise temporal and spectral

Table 2
Selected earthquakes for the dataset used in this work.

EQ No.	EQ ID[a]	F–E Region	EQ Name	EQ Country	M_w [b]	No. of records	Date	Time (UTC)
1	1406	United Kingdom	Penzance	UK	4.1*	2	10.11.1996	09:28:00
2	346	France	Epagny	France	4.2	4	15.07.1996	00:13:30
3	329	France	Grenoble	France	4.4*	10	11.01.1999	03:36:38
4	480	Switzerland	Domodossola	Italy	4	4	14.06.1993	12:28:37
5	438	Austria	Ebreichsdorf	Austria	4.1*	6	09.01.1996	01:07:22
6	1596	Austria	Bovec	Slovenia	4.3	2	06.05.1998	02:53:00
7	2144	Hungary	Varpalota	Hungary	4.7*	2	12.09.1995	22:14:04
8	34	Northern Italy	Friuli (mainshock)	Italy	6.5	24	06.05.1976	20:00:13
9	38	Northern Italy	Friuli	Italy	5.3*	2	09.05.1976	00:53:44
10	39	Northern Italy	Friuli	Italy	4.8	2	10.05.1976	04:35:54
11	40	Northern Italy	Friuli	Italy	4.9	2	11.05.1976	22:44:01
12	41	Northern Italy	Friuli	Italy	4.5*	2	13.05.1976	13:04:51
13	42	Northern Italy	Friuli	Italy	4.5*	2	15.05.1976	04:26:16
14	45	Northern Italy	Friuli	Italy	4.5*	2	18.05.1976	02:39:39
15	46	Northern Italy	Friuli	Italy	4.3*	2	01.06.1976	04:33:47
16	47	Northern Italy	Friuli	Italy	4.8*	2	01.06.1976	17:21:09
17	48	Northern Italy	Friuli	Italy	4.2	2	08.06.1976	12:14:38
18	50	Northern Italy	Friuli	Italy	4.2*	2	10.06.1976	13:04:23
19	52	Northern Italy	Friuli	Italy	5.2	4	17.06.1976	14:25:51
20	54	Northern Italy	Friuli	Italy	4.7*	4	14.07.1976	05:39:34
21	55	Northern Italy	Friuli	Italy	4.7*	2	15.07.1976	12:58:51
22	57	Northern Italy	San Gregorio	Italy	4.1	2	22.08.1976	02:49:15
23	60	Northern Italy	Friuli	Italy	5.3	10	11.09.1976	16:31:11
24	61	Northern Italy	Friuli	Italy	5.5	14	11.09.1976	16:35:03
25	62	Northern Italy	Friuli	Italy	4.8	4	13.09.1976	18:54:47
26	63	Northern Italy	Friuli	Italy	6	16	15.09.1976	03:15:19
27	64	Northern Italy	Friuli	Italy	4.9	10	15.09.1976	04:38:54
28	1205	Northern Italy	Friuli	Italy	4.7*	2	15.09.1976	04:58:42
29	65	Northern Italy	Friuli	Italy	6	28	15.09.1976	09:21:19
30	66	Northern Italy	Friuli	Italy	4.1	2	15.09.1976	09:45:54
31	72	Northern Italy	Friuli	Italy	5.4	4	16.09.1977	23:48:08
32	1823	Northern Italy	NE Gemona del Friuli	Italy	5*	4	18.04.1979	15:19:20
33	374	Northern Italy	Giaveno	Italy	4.8*	2	05.01.1980	14:32:26
34	124	Northern Italy	Toscana	Italy	4.7*	4	07.06.1980	18:35:01
35	402	Northern Italy	S of Parma	Italy	5	2	09.11.1983	16:29:52
36	403	Northern Italy	Arpiola	Italy	4.2*	2	22.03.1984	00:16:24
37	407	Northern Italy	Garfagnana	Italy	4.7*	4	23.01.1985	10:10:18
38	415	Northern Italy	NE Reggio nell'Emilia	Italy	4.9*	2	02.05.1987	20:43:54
39	477	Northern Italy	Valpelline	Italy	4.2	2	31.03.1996	06:08:02
40	1387	Northern Italy	Bovec	Slovenia	5.6	10	12.04.1998	10:55:33
41	1597	Northern Italy	Trasaghis-Friuli	Italy	4.3*	2	28.05.1998	09:39:19
42	989	Northern Italy	Cresta di Reit	Switzerland	4.9	8	29.12.1999	20:42:34
43	2169	Northern Italy	Meran	Italy	4.8	2	17.07.2001	15:06:12

[a] EQ ID is the earthquake identification used by the ISESD database.
[b] Earthquake magnitudes labelled with an asterisk have been estimated according to Section 2.2.

non-stationarities are fitted to the dataset of accelerograms. Such functional parameters are then regressed against few variables of interest for SPRA, namely, earthquake magnitude, distance-to-site and type of soil. This enables a set of predictive equations for the functional parameters to be obtained. The proposed predictive equations can be used to simulate sets of two-component horizontal accelerograms for SPRA of structures.

3.1. Mathematical formulation

Complete details of the mathematical formulation of the fully non-stationary stochastic process used in this work can be found in Rezaeian and Der Kiureghian [2]. This section provides a summary of the model and an example of its application. Rezaeian and Der Kiureghian [1] used the stochastic model proposed earlier to fit parameters to a dataset of accelerograms from Western United States. This paper is referenced, although several changes are considered in this work.

The stochastic model is based on a time-modulated filtered white-noise process with the filter having time-varying properties. It requires a time-modulating function to achieve temporal non-stationarity, and a filter function with time-varying properties to achieve spectral non-stationarity. The fully non-stationary stochastic model, $x(t)$, in its continuous form, is defined as follows:

$$x(t) = q(t,\underline{\alpha})\left[\frac{1}{\sigma_f(t)}\int_{-\infty}^{t} h[t-\tau,\underline{\lambda}(\tau)]\, w(\tau)\, d\tau\right] \tag{1}$$

where $q(t,\underline{\alpha})$ is the time-modulating function in which $\underline{\alpha}$ is a vector of parameters that control the shape and intensity of the function; $h[t-\tau,\underline{\lambda}(\tau)]$ is the linear filter with time-varying parameters $\underline{\lambda}(\tau)$; $w(\tau)$ is a white-noise (Gaussian zero-mean) process; and $\sigma_f^2(t) = \int_{-\infty}^{t} h^2[t-\tau,\underline{\lambda}(\tau)]d\tau$ is the variance of the process defined by the integral in Eq. (1). In this work, $q(t,\underline{\alpha})$ is presented as a piece-wise modulating function to model the temporal non-stationarity:

$$q(t,\underline{\alpha}) = \begin{cases} 0 & \text{if } t \le T_0 \\ \alpha_1\left(\frac{t-T_0}{T_1-T_0}\right)^2 & \text{if } T_0 < t \le T_1 \\ \alpha_1 & \text{if } T_1 < t \le T_2 \\ \alpha_1 \cdot e^{-\alpha_2(t-T_2)^{\alpha_3}} & \text{if } t > T_2 \end{cases} \tag{2}$$

Although other functions are available (e.g. gamma-type functions), the time-modulating function defined in Eq. (2) was chosen to give flexibility to the definition of the starting time and duration of the strong-shaking phase of accelerograms. This function has six parameters: $\underline{\alpha} = (\alpha_1, \alpha_2, \alpha_3, T_0, T_1, T_2)$ in which α_1 controls the maximum intensity, α_2 and α_3 are shape controllers of the decaying intensity, T_0 is the beginning of the process, and finally, T_1 and T_2 represent the start and end time of the strong shaking phase of an accelerogram. The time-varying linear filter proposed by Rezaeian and Der Kiureghian [1,2] is used in this work:

$$h[t-\tau,\underline{\lambda}(t)] = \begin{cases} \frac{\omega_f(t)}{\sqrt{1-\xi_f^2(t)}} e^{[-\xi_f(\tau)\omega_f(\tau)(t-\tau)]} \sin\left[\omega_f(\tau)\sqrt{1-\xi_f^2(\tau)}(t-\tau)\right]; & \tau \le t \\ 0; \quad \text{otherwise} \end{cases} \tag{3}$$

This filter represents the pseudo-acceleration response of a single-degree-of-freedom linear oscillator subjected to a unit impulse, in which $\tau$is the time of the pulse. In Eq. (3), the vector of parameters of the linear filter is $\underline{\lambda}(\tau) = [\omega_f(\tau), \xi_f(\tau)]$, in which $\omega_f(\tau)$ is the frequency function defining the distribution of the predominant frequency within the accelerogram, and $\xi_f(\tau)$ is the damping function controlling the bandwidth of the process. As it is expected that the predominant frequencies decay with time [60], a simple and reasonable model to consider for the frequency function is a linear decaying model:

$$\omega_f(\tau) = \omega_0 - (\omega_0 - \omega_n)\frac{\tau}{t_n} \tag{4}$$

where ω_0 and ω_n are the frequencies at the beginning and end of the accelerogram, and t_n is the total duration of the record. Although the bandwidth of accelerograms is expected to increase with time [60], as a first approximation, this variation in bandwidth can be considered to be fairly insignificant [2]. Therefore, a constant damping function is used in this work; i.e.

$$\xi_f(\tau) = \xi_f \tag{5}$$

Consequently, the fully non-stationary stochastic filtered white-noise process can be completely defined by nine parameters $(\alpha_1, \alpha_2, \alpha_3, T_0, T_1, T_2, \omega_0, \omega_n, \xi_f)$. Such parameters can be calibrated for a single recorded accelerogram and then be used to generate as many stochastic simulations as required which are compatible with the real record. In any case, artificially simulated accelerograms are likely to lead to overestimates of structural response at long structural periods [61]. In order to correct this issue, a high-pass filter is required to adjust the low-frequency content of the stochastic simulations. The high-pass filter used in this work is the second-order critically damped oscillator [60]:

$$\ddot{z}(t) + 2\omega_c\dot{z}(t) + \omega_c^2 z(t) = \ddot{x}(t) \tag{6}$$

In Eq. (6), $\ddot{z}(t)$ is the simulated (corrected) stochastic accelerogram and ω_c is the so-called "corner frequency" whose value depends upon the earthquake magnitude, the faulting geometry and the shear wave velocity [62]. The procedure to calibrate the nine parameters is briefly described through an example in the next section.

3.2. Example of simulation of accelerograms

The target accelerogram selected for this example is the North-South component of the Friuli earthquake, Northern Italy, which occurred on 06.05.1976, with a magnitude M_w 6.5, recorded in stiff soil at the Codroipo station with an epicentral distance of 42 km. The target accelerogram is shown in Fig. 3a.

- Time-modulating function parameters

The parameters $\underline{\alpha} = (\alpha_1, \alpha_2, \alpha_3, T_0, T_1, T_2)$ are determined by matching the cumulative energy of the target accelerogram, $E_a(t) = \int_0^{t_n} a^2(\tau)\, d\tau$, with the expected cumulative energy of the time-modulating function, $E_x(t) = \int_0^{t_n} q^2(\tau,\underline{\alpha})\, d\tau$. This was done through a Monte Carlo simulation approach. The parameters obtained for the target accelerogram are: $\alpha_1 = 0.232$ m/s^2, $\alpha_2 = 0.797$ s^{-1}, $\alpha_3 = 0.247$, $T_0 = 0.114$ s, $T_1 = 5.07$ s and $T_2 = 16.3$ s. Fig. 3a shows the target accelerogram and the time modulating function obtained using these parameters. Fig. 3b shows the cumulative energy for both functions and how closely they are matched. The error ε_q, in the approximation is obtained by calculating $\varepsilon_q = \int_0^{t_n} |E_x(t) - E_a(t)|dt / \int_0^{t_n} E_a(t)dt$. The error obtained for the sample accelerogram is$\varepsilon_q = 2.27\%$.

- Time-varying linear filter parameters

The iterative approach proposed by Rezaeian and Der Kiureghian [2] to obtain $\omega_f(\tau)$ and $\xi_f(\tau)$ is used. Such a procedure makes use of the *cumulative count of zero-level up-crossings* (Fig. 4a) and the *cumulative count of positive minima and negative maxima* (Fig. 4b) as surrogates of the predominant frequency and bandwidth, respectively. This procedure was done through a Monte Carlo simulation approach. Five damping ratios are considered for this example: $\xi_f = 0.25$, 0.30, 0.35, 0.40 and 0.45. The matching errors between the target and stochastic processes, both

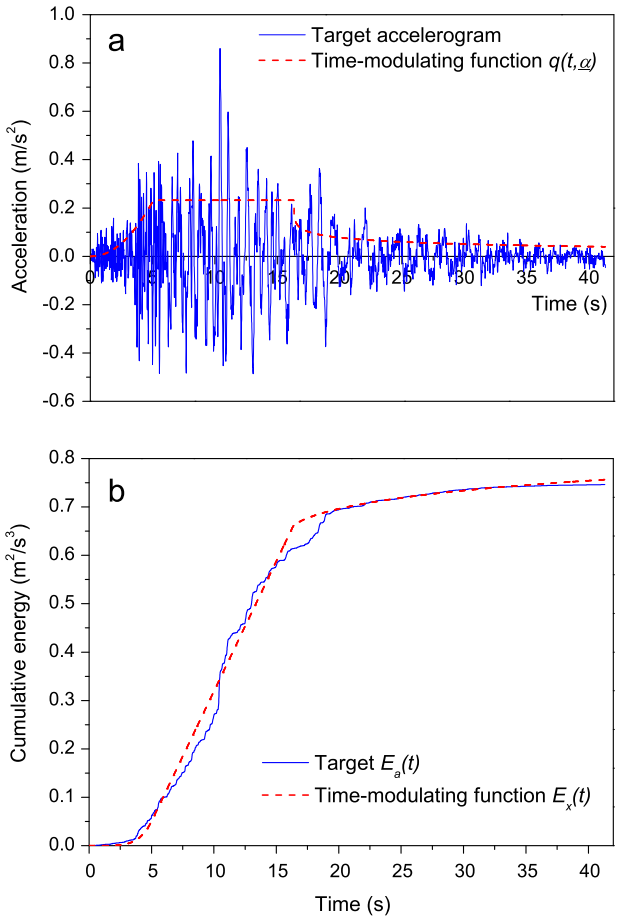

Fig. 3. Time-modulating function fitting process. (a) Target accelerogram and time-modulating function. (b) Cumulative energy for the target accelerogram and time-modulating function.

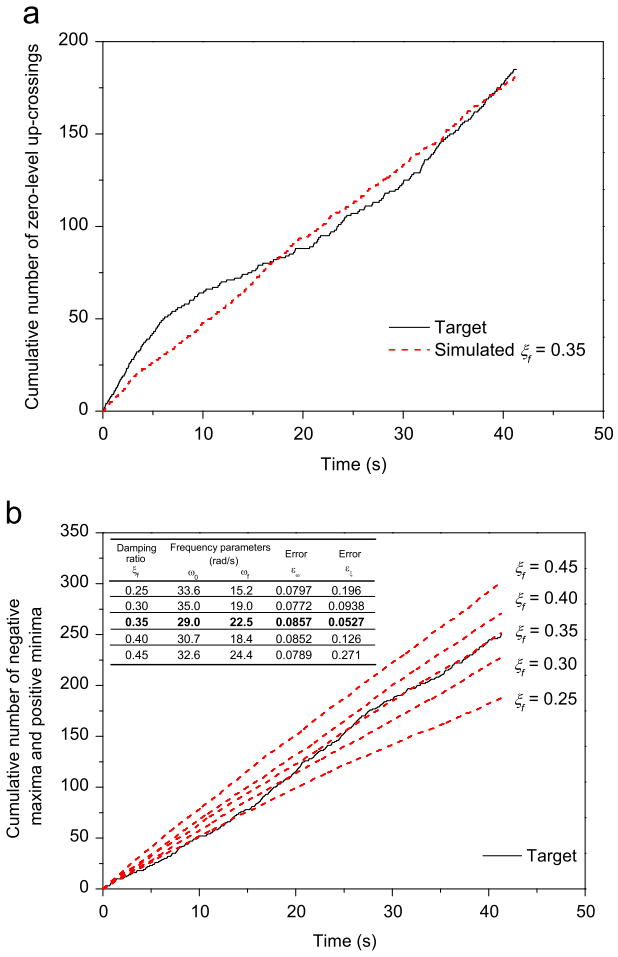

Fig. 4. Time-varying linear filter fitting process. (a) Cumulative number of zero-level up-crossings. (b) Cumulative number of negative maxima and positive minima.

in the cumulative number of zero-level up-crossings, ε_ω, and the cumulative count of positive minima and negative maxima, ε_ξ, can be obtained by minimising the difference between the curves normalised by the target curve. These errors are summarised in Fig. 4b for each damping ratio. The controlling error ε_ξ is minimised for the following filter parameters: frequency function parameters of $\omega_0 = 29.0$ rad/s,$\omega_f = 22.5$ rad/s with a damping ratio of $\xi_f = 0.35$.

Using the nine parameters determined above, it is possible to obtain as many accelerogram simulations as desired, which are compatible with the features of the target accelerogram. Each simulation is based on a different random white-noise process that gives a stochastic character to the model. Fig. 5 shows two simulations obtained and the target accelerogram.

Fig. 6a shows a comparison of 5% damped spectral acceleration for 10 simulated ground-motions and the recorded accelerogram. From this figure, it is possible to observe that at long periods, the simulated accelerograms are systematically above the target response spectrum. The high-pass filter defined in Eq. (6) with a corner frequency of $\omega_c = \pi$ (rad/s) is used to adjust the low-frequency content of the stochastic simulations. From Fig. 6b it can be seen that the post processing reduces the fitting error between the simulations and the target accelerogram in the long-period range without affecting the short/medium-period ranges.

In the next section, the nine functional parameters that define the stochastic process will be obtained for each of the accelerograms in the dataset defined in Section 2.

3.3. Model calibration

The two horizontal components of simulated ground motion accelerograms have to be orientated consistently in terms of their energy content to allow the structural engineer to make reasonable estimations of nonlinear structural responses. A minor setback of the dataset of accelerograms described in Section 2 is that their orientations are arbitrary and depend on the orientation of the recording instruments. Therefore, the dataset needs to be standardised to make reliable simulations. In this work, the dataset's standardisation was undertaken by orientating the two horizontal components into their *principal axes*. In such a scenario, the two components are uncorrelated, facilitating the simulation of suitable components of horizontal accelerograms for structural engineering purposes.

3.3.1. Principal axes

Earthquake ground motions could be orthogonally rotated along their principal axes, in which their intensities are maximum, intermediate and minimum with zero covariances [63]. Consequently, simulated earthquake accelerograms did not need to be statistically correlated when their components were orientated in their principal axes [64]. In general, the major principal component points to the earthquake epicentre, the intermediate principal component is perpendicular to the major component, and the minor principal component is vertical. In this work, the major and intermediate components for each of the selected 110 pairs of

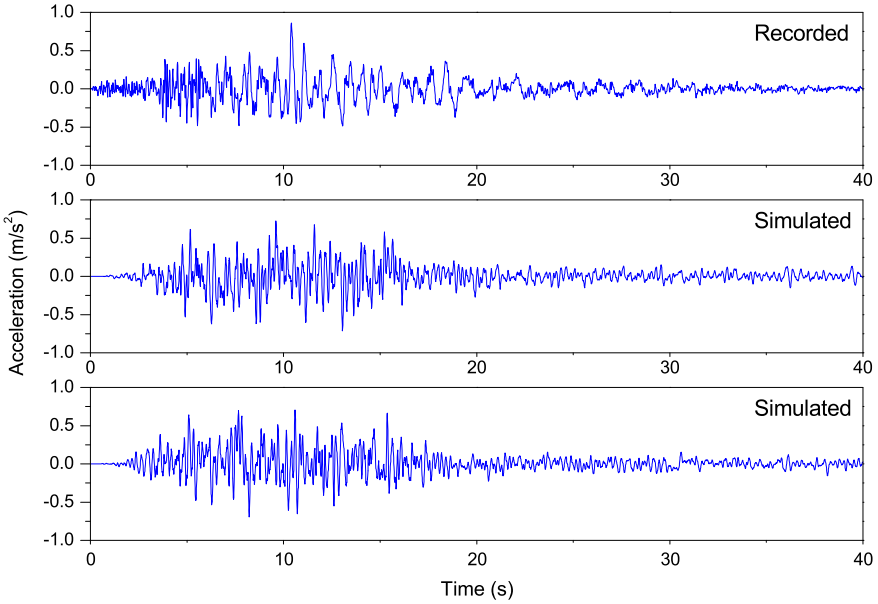

Fig. 5. Target accelerogram and two simulations using the stochastic model.

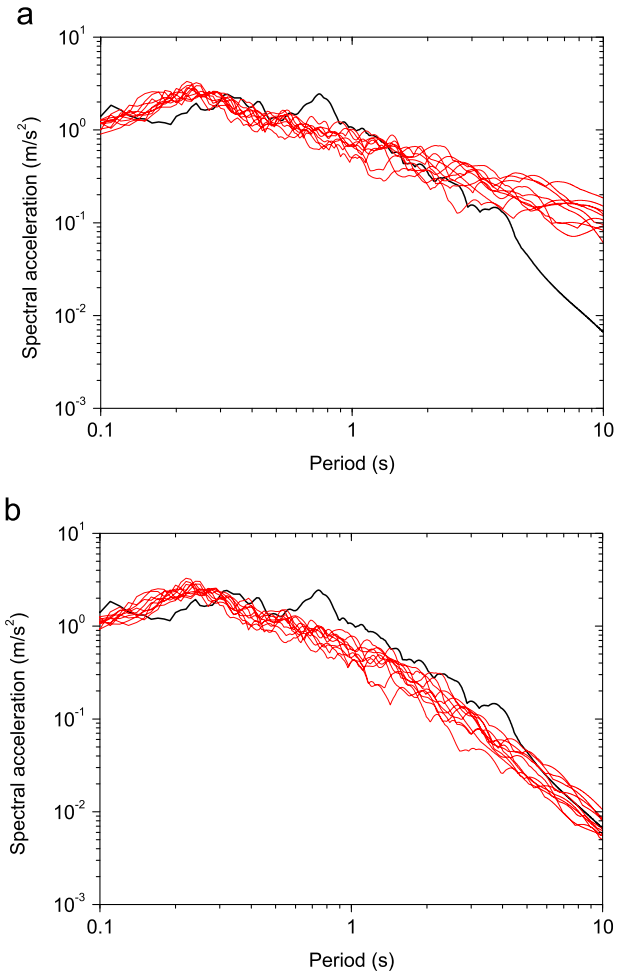

Fig. 6. Acceleration response spectra of the target accelerogram (the thick black line) and 10 simulations (the thin red lines). (a) Before high-pass filtering. (b) After high-pass filtering (For interpretation of the references to color in this figure legend, the reader is referred to the web version of this article.).

accelerograms are estimated. Then, the nine parameters of the stochastic process are fitted to each rotated accelerogram. In this light, such parameter values are associated to two uncorrelated horizontal ground motion components, i.e. the major and intermediate components. The vertical component is not included, although it could be incorporated in future models. When two horizontal ground motion components, $a_i(t)$ and $a_j(t)$, are orientated along their principal axes, their correlation coefficient, ρ_{ij}, is zero [65]. A qualitative measurement used to discriminate between the maximum and intermediate component is the Arias intensity [63], which is a measure of the total energy contained in an accelerogram. Naturally, the major component has the larger Arias intensity and the intermediate component has the smaller Arias intensity. Consequently, each of the 110 pairs of accelerograms was orthogonally rotated until the correlation coefficient reached a zero value (or a numerically small number). In this way, all pairs of accelerograms of the dataset were orientated in their major and intermediate principal components, using the Arias intensity as the discerning criterion. After rotation, the nine parameters of the stochastic process were calibrated for each accelerogram following the procedure discussed in Section 3.2. Table 3 gives a statistical summary of the nine parameters for both principal components.

In order to test the appropriateness of the numerical values for the parameters selected to simulate the major and intermediate components of accelerograms, four recorded bi-axial accelerograms from the dataset were selected to compare them against simulated records. Such accelerograms are identified using the unique waveform ID given by the ISESD database. They correspond to the following events: (1) M_w 6, R_{epi}=32 km (ID: 140); (2) M_w 4, R_{epi}=40 km (ID: 1338); (3) M_w 6.5, R_{epi}=42 km (ID: 49); and (4) M_w 4.7, R_{epi}=15 km (ID: 259). Accelerograms (1) and (2) were recorded in rock conditions whereas (3) and (4) were recorded in stiff soil conditions. Fig. 7 shows the major and intermediate components of the recorded accelerograms and corresponding stochastic simulations using the procedure summarised in Section 3.2.

3.3.2. *Distribution fitting*

For simplicity, some results presented in this section are for the major principal component only; however, when necessary for the completeness of the model, results for the intermediate component are included. To assign one statistical distribution for each parameter

of the stochastic process, their corresponding histograms were obtained. Then, trial marginal distributions were fitted to the corresponding histograms using the maximum likelihood estimation technique. To select the marginal distribution that best fits the corresponding histogram, the Kolmogorov–Smirnov goodness-of-fit test and the standard p-value used in statistical hypothesis testing were calculated for decision-making. All marginal distributions tested and selected were taken from the MATLAB's statistical toolbox. Fig. 8 shows the normalised histograms for each parameter of the stochastic process for the major component of the accelerogram dataset. Table 4 summarises the governing parameters obtained for the fitted marginal distributions and their p-values. From this table it can be seen that all marginal distributions selected are accepted (or more precisely, all null hypotheses stating that the experimental data for each parameter following the assigned marginal distribution fail to be rejected) at the standard 0.05 significance level. Furthermore, the remarkably high p-values confirm the high likelihood that the measured data actually come from the selected marginal distributions.

Table 3
Summary of parameters of the stochastic process for the major and intermediate components for the 220 accelerograms.

Major Component					
Parameter	Minimum	Maximum	Mean	Standard deviation	Coefficient of variation
α_1 (m/s^2)	0.000235	1.70	0.201	0.344	1.71
α_2 (s^{-1})	0.0353	3.10	0.818	0.491	0.600
α_3 (unitless)	0.0128	3.32	0.522	0.405	0.776
T_0 (s)	0.00440	13.0	1.87	2.87	1.53
T_1 (s)	0.0890	30.0	4.73	6.37	1.34
T_2 (s)	0.219	39.0	6.81	7.52	1.10
ω_0 (rad/s)	16.6	122.2	53.6	21.9	0.409
ω_n (rad/s)	1.35	87.0	31.7	18.3	0.576
ξ (ratio)	0.0600	0.800	0.242	0.126	0.519
Intermediate component					
α_1 (m/s^2)	0.000218	2.35	0.188	0.281	1.50
α_2 (s^{-1})	0.0703	2.28	0.788	0.438	0.556
α_3 (unitless)	0.0177	1.35	0.516	0.271	0.525
T_0 (s)	0.00400	12.9	1.80	2.65	1.47
T_1 (s)	0.0959	32.0	4.81	6.63	1.38
T_2 (s)	0.247	35.6	6.76	7.51	1.11
ω_0 (rad/s)	13.6	116.2	53.9	22.2	0.411
ω_n (rad/s)	1.22	80.8	32.4	19.4	0.598
ξ (ratio)	0.0600	0.800	0.248	0.147	0.592

3.3.3. *Regression analysis*

In this section, empirical predictive equations are proposed for each of the nine parameters. These predictive equations were obtained by means of regression analysis and a functional form is proposed to explain the statistical behaviour of each parameter (dependent variable) as a function of earthquake moment magnitude (M_w), epicentral distance (R_{epi}) and type of soil (independent variables). However, when assessing the significance of the regressions, the errors are assumed to be normally distributed for the functional form to be statistically meaningful. This statement implies that the dependent variables are also normally distributed

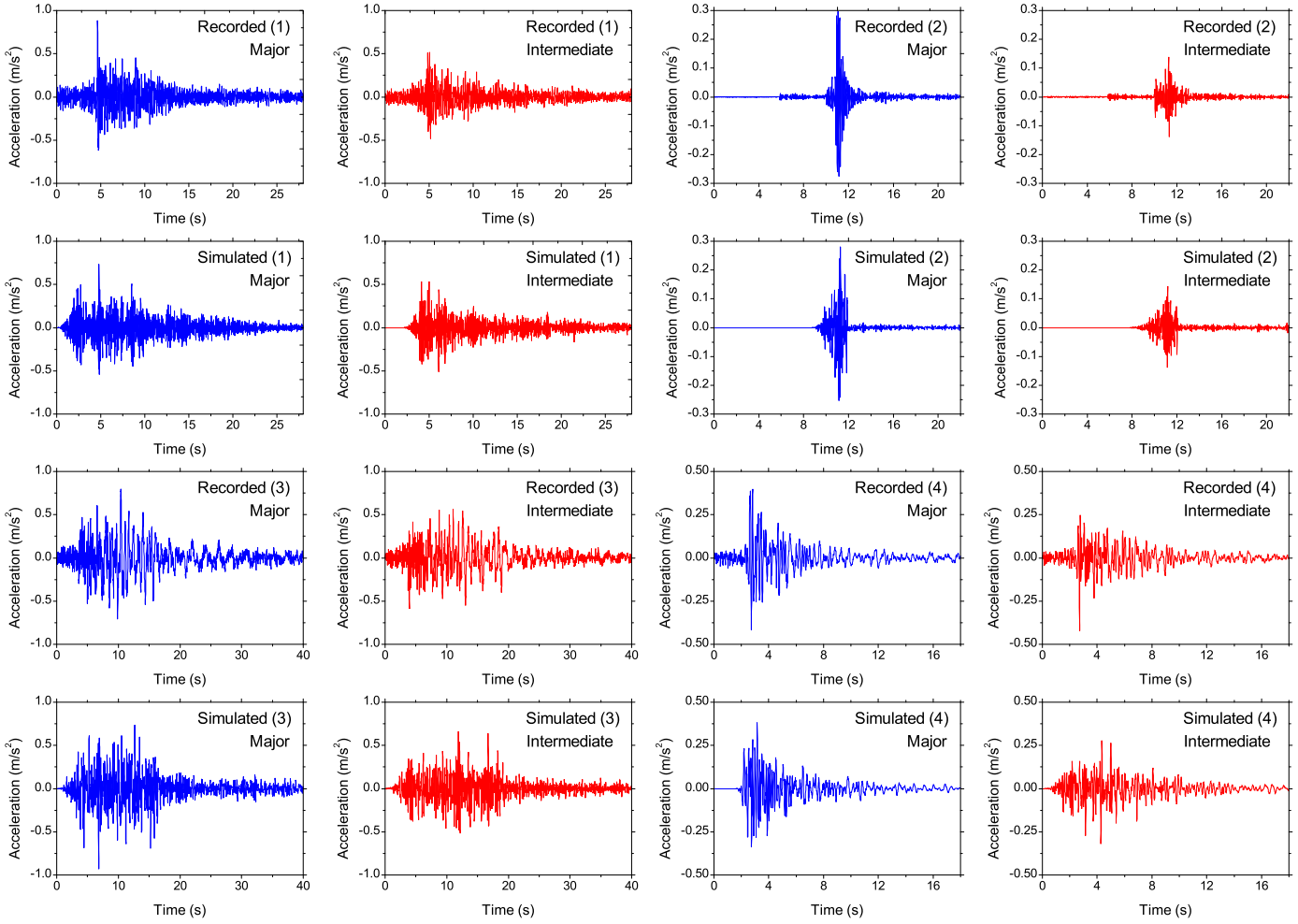

Fig. 7. Four recorded accelerograms (first and third rows) and corresponding simulations (second and fourth rows) for both principal components.

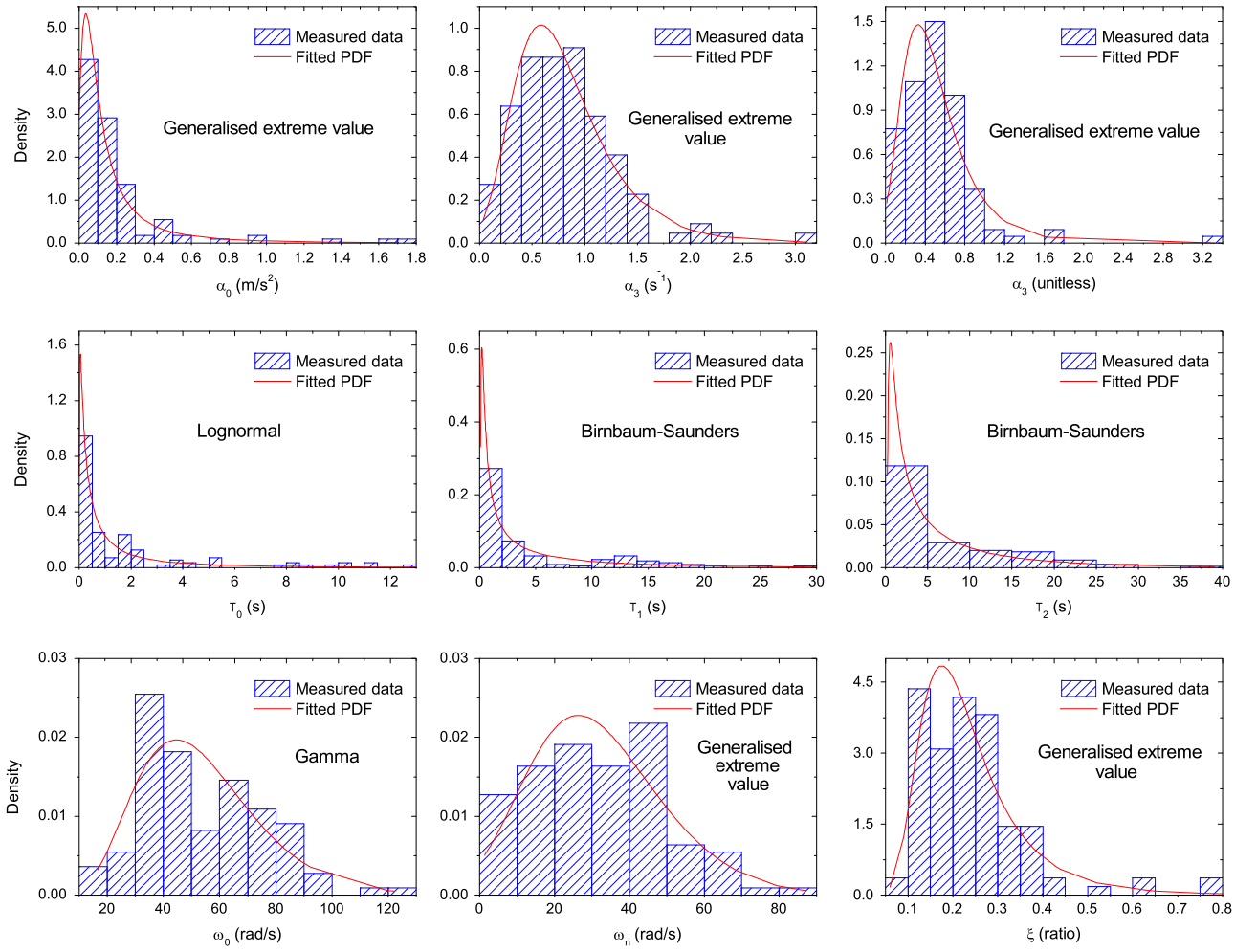

Fig. 8. Normalised histograms for each parameter of the stochastic process and their fitted marginal distributions for the major components of the accelerogram dataset.

Table 4
Fitted marginal distributions and results of hypothesis testing.

Parameter	**Fitted distribution**	Distribution parameters	Major		Intermediate	
			Value	*p*-value	Value	*p*-value
α_1 (m/s^2)	Generalised extreme value	k	0.635	0.325	0.603	0.718
		σ	0.082		0.078	
		μ	0.070		0.068	
α_2 (s^{-1})	Generalised extreme value	k	0.033	0.938	0.045	0.986
		σ	0.363		0.322	
		μ	0.597		0.587	
α_3 (unitless)	Generalised extreme value	k	0.093	0.725	−0.121	0.886
		σ	0.250		0.240	
		μ	0.353		0.403	
T_0 (s)	Lognormal	μ	−0.475	0.581	−0.433	0.833
		σ	1.664		1.570	
T_1 (s)	Birnbaum–Saunders	β	1.838	0.426	1.866	0.202
		γ	1.801		1.800	
T_2 (s)	Birnbaum–Saunders	β	3.310	0.481	3.425	0.590
		γ	1.435		1.392	
ω_0 (rad/s)	Gamma	a	6.014	0.254	5.933	0.644
		b	8.906		9.089	
ω_n (rad/s)	Generalised extreme value	k	−0.132	0.629	−0.125	0.921
		σ	16.296		17.076	
		μ	24.138		24.285	
ξ (ratio)	Generalised extreme value	k	0.143	0.889	0.214	0.983
		σ	0.077		0.084	
		μ	0.185		0.178	

[66]. However, as can be seen from Fig. 8, the dependent variables exhibit a non-normal statistical behaviour. Therefore, a transformation to the normal domain is required. The following change of variables was used [1]:

$$v_i = \Phi^{-1}\left[F_{\theta i}(\theta_i)\right] \quad i = 1, \ldots, 9 \tag{7}$$

In Eq. (7), v_i is the i-th transformed standard normal random variable; Φ^{-1} is the inverse standard normal cumulative distribution; θ_i is i-th parameter that defines the stochastic process, and $F_{\theta i}(\theta_i)$ is the marginal cumulative distribution function fitted for each θ_i. Once the nine dependent variables were transformed into normal distributions, empirical predictive equations were fitted to the measured data by means of regression analysis. As all data points of the dataset cannot be considered statistically independent observations, the random-effects regression technique by means of the algorithm proposed by Abrahamson and Youngs [67] was used to account for such an effect.

Regarding the functional form selected for the dependent variables, it is worth mentioning that models traditionally used for GMPEs are not necessarily valid for application in this work. Such models showed very little statistical significance in the regression analyses. This is due to the fact that GMPEs directly predict particular features of ground motions (e.g. peak ground acceleration) whereas the predictive equations proposed in this work determine nine single variables which are able to predict ground-motion accelerograms. As a consequence, the variable selection, and the form of such variables, played a crucial role in proposing a statistically meaningful functional form for the dependent variables. In this work, the forward stepwise method [66] was used to define the form of the variables and the functional form of the model. The main objective was to keep the number of explanatory variables as low as possible with the highest possible statistical significance, using only one functional form for all dependent variables. The functional form proposed for all parameters is given in Eq. (8), with the regression coefficients presented in Table 5.

$$v_i = \beta_{i,0} + \beta_{i,1} \cdot M_w + \beta_{i,2} \cdot \sqrt{R_{epi}} + \beta_{i,3} \cdot \ln\left(M_w \cdot R_{epi}\right) + \beta_{i,4} \cdot D_1 + \beta_{i,5} \cdot D_2 + n_i + \varepsilon_i \quad i = 1, \ldots, 9 \tag{8}$$

In Eq. (8), M_w and R_{epi} are the moment magnitude and epicentral distance (in km) for the seismic scenario to be simulated. The type of soil is modelled through two dummy variables D_1 and D_2: $D_1 = D_2 = 0$ for rock; $D_1 = 1$ and $D_2 = 0$ for stiff soil; and $D_1 = 0$ and $D_2 = 1$ for soft soil. Finally, n_i and ε_i are two normal random variables with zero mean and variances τ_i^2 and σ_i^2 that represent the residuals of the regressions for inter-event (random effect among different earthquakes) and intra-event (random effect among different accelerograms for the same earthquake) respectively. The total error of the model is then a normal random variable with zero mean and variance $\tau_i^2 + \sigma_i^2$. Table 5 also provides the standard deviations τ_i and σ_i. P-values in Table 5 are addressed in the following section.

3.3.4. Significance of regressions

In this section, the significance of the regressions are assessed for both the overall model adequacy and the coefficients obtained. Initially, the overall significance of the regression was assessed. For this case, the p-values for the f-test for the null hypothesis $H_0 : \beta_1 = \cdots = \beta_5 = 0$ are reported in Table 6. As all p-values are smaller than the standard 5% significance level, all null hypotheses are rejected. Also, the residual analysis was performed, and the total residuals were plotted against the model variables to check for deviations from normality. Figs. 9 and 10 show scatter plots of the total residuals for the nine dependent variables against M_w and R_{epi}, respectively. From this set of plots it is possible to observe that there are no apparent deviations from normality.

Tests on the significance of individual regression coefficients were also performed. P-values for the t-test for the null hypothesis $H_0 : \beta_i = 0$ are reported in Table 6 (β_0's are not included in this analysis as constants were not scrutinised).

Some p-values are higher than the standard 0.05 significance level, which means that the corresponding null hypothesis fails to be rejected. In such a case, the regression coefficients are of little value in explaining the variation of the corresponding dependent variable. However, as the functional form, in its entirety, is still able to represent the variation of the nine dependent variables (see p-values in Table 5), the regression coefficients of Table 5 were considered valid for simulations.

3.3.5. Correlations within principal axes

The variables v_i (either for the major or intermediate component) are correlated as they are derived using the same set of data, i.e. they are jointly normal random variables. Therefore, for consistency, such a correlation must be preserved when simulating

Table 5
Regression coefficients and standard deviations for the error random variables.

	Major component								
	β_0	β_1	β_2	β_3	β_4	β_5	τ	σ	p-value
v_1 (α_1)	0.7814	1.0668	0.2751	−1.6070	0.4110	0.0175	0.4852	0.5323	0.0000
v_2 (α_2)	4.1555	−0.2059	0.1435	−0.7665	−0.1218	0.2462	0.3564	0.8328	0.0008
v_3 (α_3)	0.9996	−0.0814	−0.0848	0.0069	0.0245	−0.6082	0.0781	0.9301	0.0215
v_4 (T_0)	−4.6028	−0.3342	−0.5952	1.9832	−0.2727	−0.1397	0.5740	0.7547	0.0075
v_5 (T_1)	−2.5345	−0.4945	−0.3979	1.4768	−0.0901	−0.0583	0.6754	0.7045	0.0231
v_6 (T_2)	−4.2075	−0.3931	−0.4153	1.7161	0.0544	0.0253	0.6779	0.6803	0.0114
v_7 (ω_0)	−0.7748	−0.8501	−0.4613	1.6332	−0.5170	−0.3077	0.1836	0.8411	0.0000
v_8 (ω_n)	−5.0464	−0.3083	−0.4932	1.9619	−0.6393	−0.2972	0.0141	0.8893	0.0001
v_9 (ξ)	−4.7793	−0.3850	−0.6217	2.1016	−0.2991	0.1322	0.1497	0.9501	0.0094
	Intermediate component								
v_1 (α_1)	0.5402	1.1438	0.3179	−1.6877	0.3794	−0.0083	0.4614	0.5215	0.0000
v_2 (α_2)	4.2933	−0.2351	0.2155	−0.8684	0.0720	0.1836	0.2663	1.0900	0.0081
v_3 (α_3)	1.7895	0.1881	0.0324	−0.5290	−0.3243	−0.6067	0.0374	0.9414	0.0353
v_4 (T_0)	−3.2093	−0.3599	−0.4034	1.5237	−0.4577	−0.0341	0.4960	0.8228	0.0255
v_5 (T_1)	−1.3461	−0.4227	−0.2670	1.0069	0.0036	−0.0502	0.8223	0.5098	0.0407
v_6 (T_2)	−4.7822	−0.4157	−0.5005	1.9481	0.0585	0.0649	0.7318	0.6281	0.0058
v_7 (ω_0)	0.1198	−0.7409	−0.3740	1.2472	−0.5771	−0.4125	0.2953	0.7965	0.0000
v_8 (ω_n)	−5.4575	−0.4664	−0.5289	2.2222	−0.4059	−0.2255	0.1628	1.0345	0.0000
v_9 (ξ)	−1.8771	−0.5859	−0.3816	1.4128	0.0405	0.3150	0.0640	0.9628	0.0194

Table 6
P-values for the *t*-test for the null hypothesis $H_0 : \beta_i = 0$.

	Major component					Intermediate component				
	β_1	β_2	β_3	β_4	β_5	β_1	β_2	β_3	β_4	β_5
ν_1 (α_1)	0.000	0.031	0.000	0.014	0.936	0.000	0.010	0.000	0.019	0.969
ν_2 (α_2)	0.202	0.367	0.167	0.558	0.370	0.239	0.275	0.206	0.780	0.589
ν_3 (α_3)	0.623	0.605	0.990	0.909	0.033	0.262	0.845	0.358	0.136	0.035
ν_4 (T_0)	0.049	0.001	0.001	0.212	0.626	0.037	0.018	0.010	0.040	0.907
ν_5 (T_1)	0.005	0.022	0.014	0.688	0.843	0.015	0.118	0.090	0.987	0.864
ν_6 (T_2)	0.023	0.015	0.004	0.805	0.931	0.017	0.004	0.001	0.792	0.824
ν_7 (ω_0)	0.000	0.003	0.002	0.010	0.239	0.000	0.013	0.018	0.004	0.110
ν_8 (ω_n)	0.053	0.002	0.000	0.002	0.270	0.013	0.005	0.001	0.094	0.477
ν_9 (ξ)	0.026	0.000	0.001	0.177	0.650	0.001	0.026	0.018	0.855	0.282

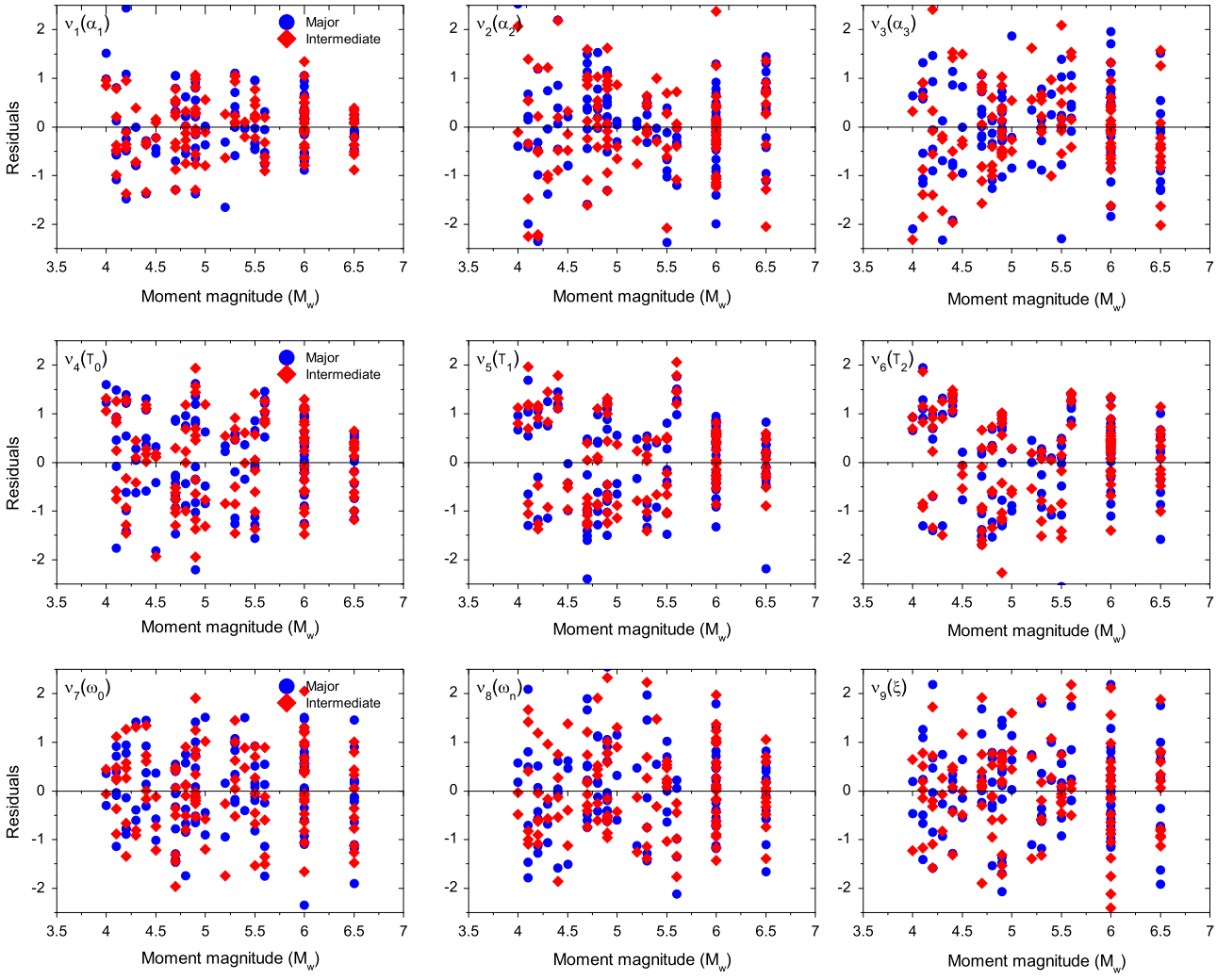

Fig. 9. Scatter plots of residuals against moment magnitude for the nine normalised variables.

accelerograms using the stochastic model and the predictive equations obtained from the regressions. This correlation can be estimated as the correlation coefficient between the inter-event η_i and the intra-event ε_i components of the total residual of regressions [1]. Table 7 shows the matrices of correlation coefficients for variables v_i for the major and intermediate components.

4. Simulation of accelerograms and model validation

In this section, the stochastic ground motion accelerogram model described in Section 3 is used to simulate accelerograms in order to validate its application against recorded accelerograms and GMPEs. The procedure involved in the generation of artificial accelerograms for any seismic scenario (moment magnitude, epicentral distance and type of soil) is summarised. Then, simulated accelerograms are compared with recorded accelerograms from the dataset. From this comparison, it is possible to see that the model is able to simulate the natural variability of accelerograms in terms of intensity, frequency content and time duration for a defined seismic scenario. In this sense, a recorded accelerogram can be seen as one data point from a wider range of accelerograms possible to be generated under a particular seismic

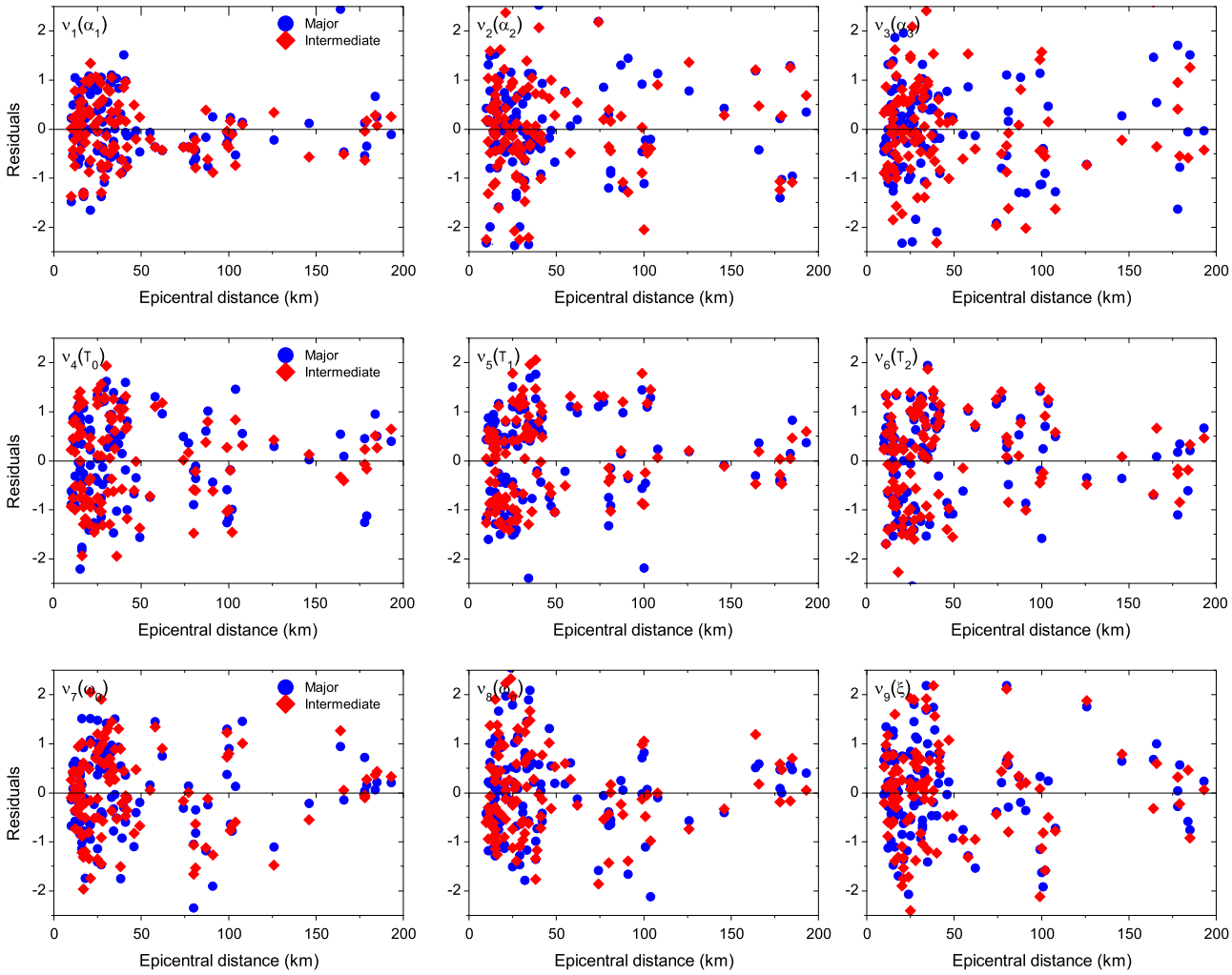

Fig. 10. Scatter plots of residuals against epicentral distance for the nine normalised variables.

Table 7
Correlation coefficients matrices for variables v_i for the major and intermediate component.

	Major component								
	$v1$	$v2$	$v3$	$v4$	$v5$	$v6$	$v7$	$v8$	$v9$
$v1$	1								
$v2$	0.4049	1							
$v3$	0.1551	−0.4909	1					Sym	
$v4$	−0.095	−0.0811	0.2381	1					
$v5$	−0.1872	−0.1506	0.2655	0.7648	1				
$v6$	−0.3815	−0.1849	0.1728	0.6766	0.883	1			
$v7$	0.081	−0.0557	0.0935	0.415	0.3592	0.2766	1		
$v8$	0.1741	−0.0108	0.0755	−0.1476	−0.1823	−0.2478	0.0998	1	
$v9$	−0.1388	−0.1155	0.0657	0.0959	−0.0167	−0.0003	−0.2352	−0.1544	1
	Intermediate component								
$v1$	1								
$v2$	0.479	1							
$v3$	0.095	−0.549	1						
$v4$	−0.093	−0.117	0.176	1				Sym	
$v5$	−0.235	−0.160	0.200	0.734	1				
$v6$	−0.379	−0.226	0.095	0.625	0.892	1			
$v7$	0.185	−0.048	0.258	0.405	0.366	0.308	1		
$v8$	0.195	0.091	0.050	−0.164	−0.180	−0.185	0.218	1	
$v9$	−0.252	−0.038	−0.068	0.097	0.013	0.021	−0.312	−0.337	1

scenario. A comprehensive set of accelerograms can be simulated containing as many accelerograms as required by the structural engineer to use for nonlinear time-history analyses. The model is validated in terms of peak ground acceleration, peak ground velocity and spectral accelerations. Accelerograms were simulated using the model proposed for a wide range of seismic scenarios

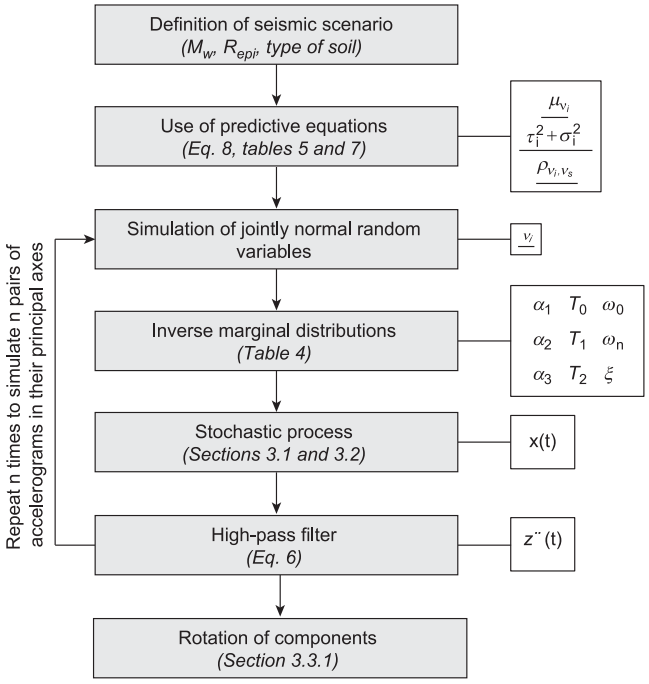

Fig. 11. Flowchart for the simulation of accelerograms compatible with a particular seismic scenario using the proposed model.

and compared with predictions made by GMPEs. The attenuation relations selected for these comparisons can be grouped in three main categories: (i) the UK, as a particular application of NW Europe, (ii) the broader region of Europe and the Middle East, and (iii) other Stable Continental Regions (SCRs) that possess a similar tectonic behaviour as NW Europe. The objective is to analyse the predictions made with the proposed model when compared with GMPEs whose target geographical regions can be considered comparable, to some extent, to the target region in this work.

4.1. Simulation of accelerograms

The flowchart in Fig. 11 summarises the steps to simulate accelerograms compatible with a particular seismic scenario (moment magnitude, epicentral distance and type of soil).

The procedure described in Fig. 11 was used to simulate accelerograms using a sample of four scenarios from the dataset outlined in Section 3.3, namely, the following events: (1) M_w 6, R_{epi}=32 km (ID: 140); (2) M_w 4, R_{epi}=40 km (ID: 1338); (3) M_w 6.5, R_{epi}=42 km (ID: 49); and (4) M_w 4.7, R_{epi}=15 km (ID: 259).

4.2. Validation for recorded accelerograms

Figs. 12 and 13 show the recorded traces of acceleration, velocity and displacement corresponding to the events selected that were recorded in rock condition and stiff soil conditions, respectively, and three stochastic simulations for each event. These figures show that for a single seismic scenario, a great variability in terms of intensity, frequency content and duration of the strong shaking phase is present in the simulated accelerograms. Such variability is likely to have a significant effect when assessing the seismic risk of civil structures for seismic scenarios of interest that dictate the seismic hazard of the selected site. Certainly, for structural engineering analyses, the zero acceleration history that may be obtained at the beginning of simulated accelerograms can be truncated to avoid unnecessary use of computer resources.

Fig. 14 shows the 5% damped acceleration response spectra for 30 simulations for the major component of each accelerogram defined above plus the response spectra for the four major components of the real records. It is observed that real accelerograms can be considered as only one record likely to be generated under the seismic scenario analysed. The variability present in the response spectra can be regarded as the natural variability associated with the earthquake generation phenomenon. Such variability should be properly accounted for when defining the seismic input for seismic probabilistic risk analysis. For NW European earthquakes, the proposed model seems to characterise reasonably well the natural variability of earthquakes for different scenarios defined by magnitudes, distances and types of soil.

4.3. Validation for GMPEs

4.3.1. Selection of GMPEs

A total of 15 GMPEs were selected for the three groups of comparisons, namely, (i) the UK, (ii) Europe and Middle East and (iii) other SCRs. Table 8 summarises these GMPEs and their main characteristics.

The following assumptions are made in order to perform meaningful comparisons between the GMPEs in Table 8 and the proposed model.

4.3.1.1. Scale magnitude. The moment magnitude scale (M_w) is used for the comparisons. GMPEs calibrated using the local magnitude (M_L) and the surface-wave magnitude (M_s) are transformed to M_w using the formulae calibrated by Johnston [49] for SCRs.

4.3.1.2. Distance metric. The epicentral distance (R_{epi}) is used for the comparisons. In order to allow transformations to R_{epi} from GMPEs calibrated using the Joyner–Boore distance (R_{JB}), hypocentral distance (R_{hyp}) and the rupture distance (R_{rup}), the following three assumptions are made: (i) only vertical faults are considered: in such a case, $R_{JB}=R_{epi}$; (ii) the focal depth is fixed to h=15 km; hence, the relationship between R_{epi} and R_{hyp} is analytical $\left(R_{hyp}=\sqrt{R_{epi}^2+h^2}\right)$ and (iii) the earthquake rupture is modelled as a point source: in such a case $R_{rup}=R_{hyp}$ and assumption (ii) can then be applied. It is worth mentioning that such a focal depth can be considered "average" for British earthquakes (Musson [52] provided a discussion on the focal depths for UK earthquakes) and it was also used by other researchers (e.g. the GMPE of Dahle et al. [73] for intraplate regions).

4.3.1.3. Type of soil. Comparisons are made either considering rock or hard rock conditions. Therefore, conversion factors between both types of soil are used. In any case, a rigorous adjustment would involve knowledge of the soil profile of the site of interest in terms of both shear-wave velocity and soil density [80]. As a rough estimation is intended in the following sections, simplified approaches are followed. One such approach, Cotton et al. [81], provided adjustment factors for hard rock conditions (V_{S30}=2880 m/s) and rock conditions (V_{S30}=618 m/s). A more recent model reported by Van Houtte et al. [82] provided adjustment factors derived for hard rock sites ($V_{S30}>2000$ m/s) and rock sites ($V_{S30}\sim800$ m/s). Either model could be used, however, the adjustment factors proposed by Van Houtte et al. [82] are arbitrarily selected. For those GMPEs that did not include site classification, it is assumed that they were calibrated for generic rock conditions, unless otherwise stated.

4.3.1.4. Style of faulting. GMPEs that include the style of faulting are set to strike-slip conditions. Even though the proposed model does not include style of faulting, strike-slip condition is chosen as it is most likely to occur in British earthquakes [31].

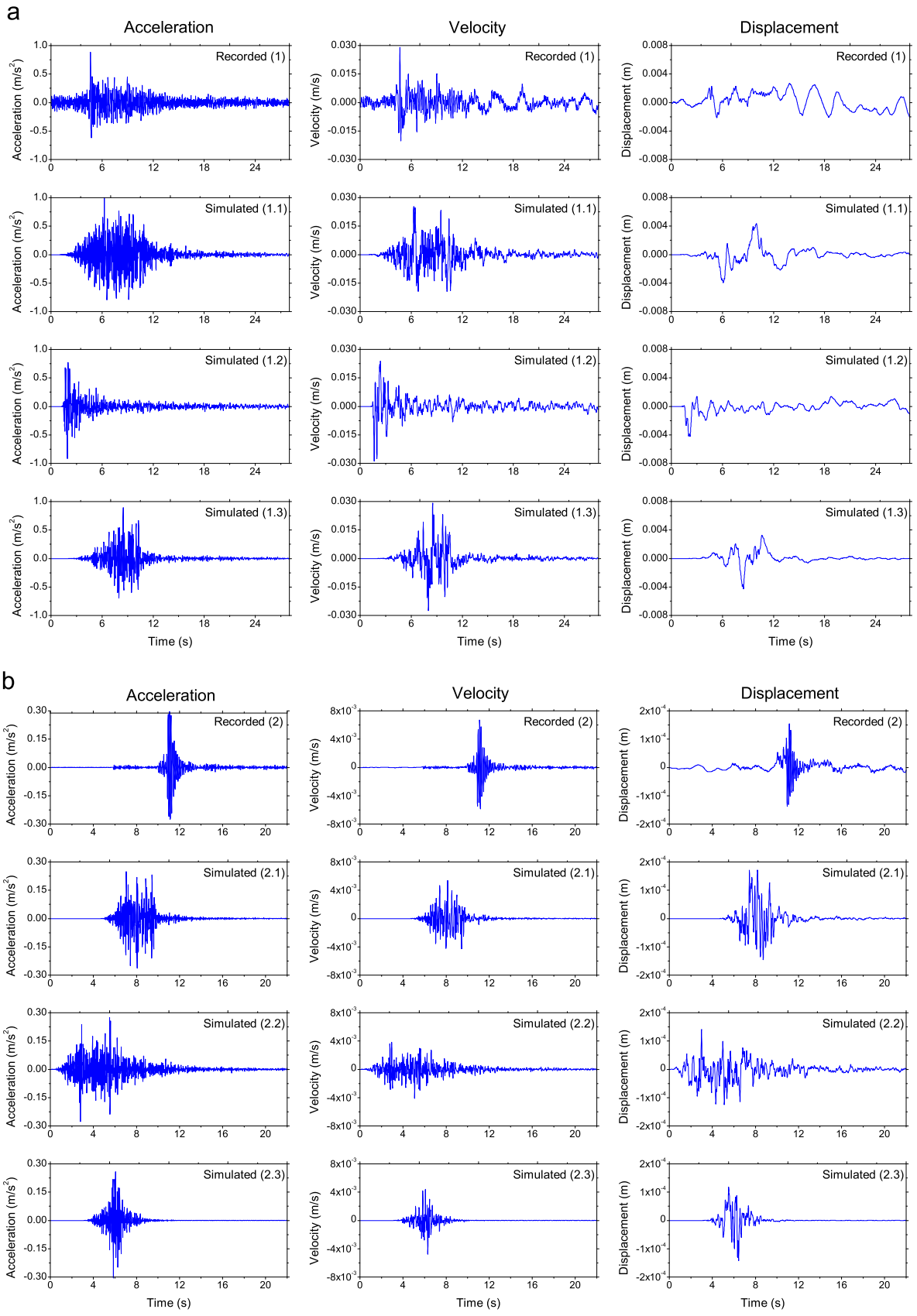

Fig. 12. Recorded (first row) and simulated traces (last three rows) of acceleration, velocity and displacement recorded in rock conditions. (a) M_w 6, R_{epi}=32 km (ID: 140). (b) M_w 4, R_{epi}=40 km (ID: 1338).

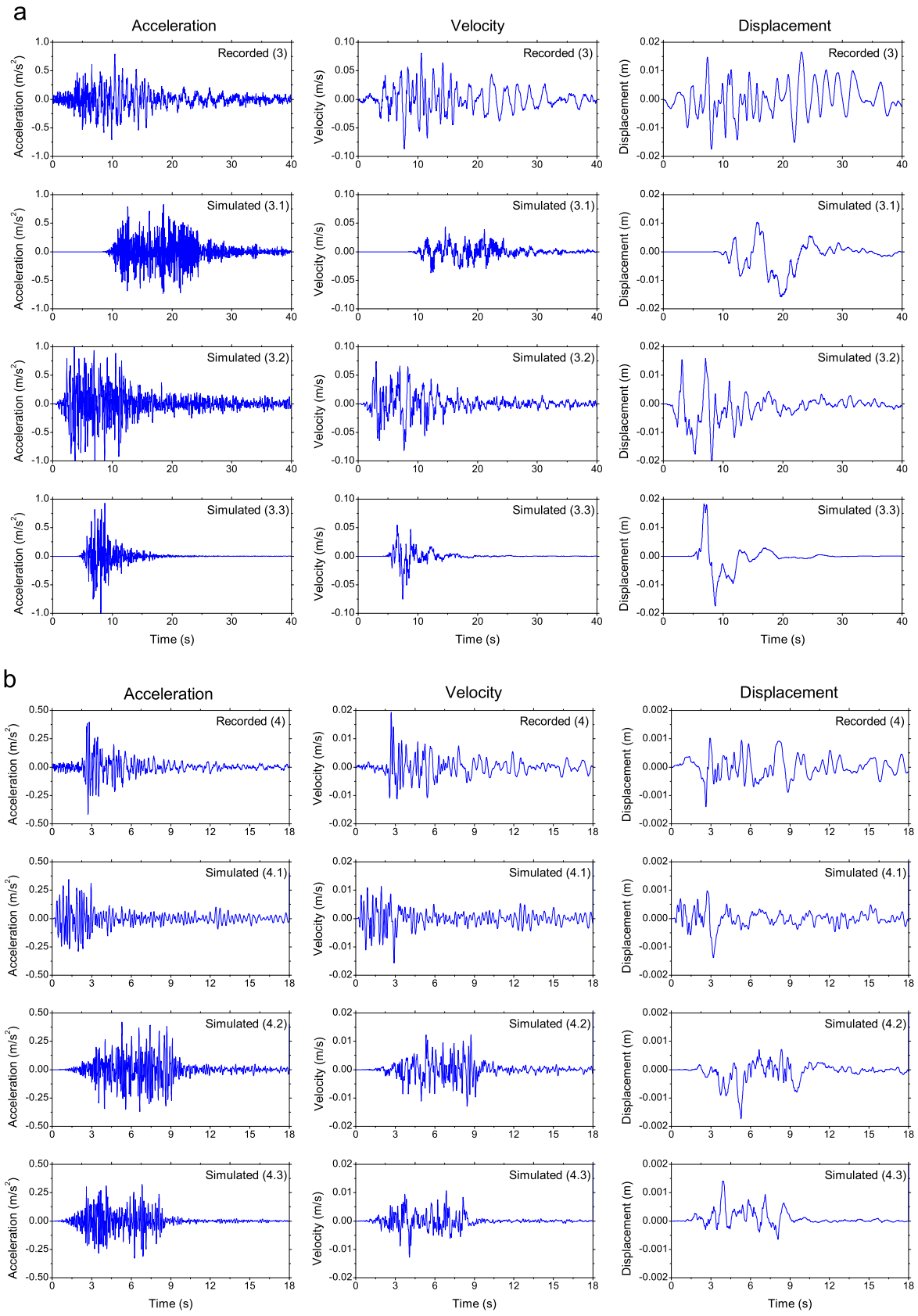

Fig. 13. Recorded (first row) and simulated traces (last three rows) of acceleration, velocity and displacement recorded in stiff soil conditions. (a) M_w 6.5, R_{epi}=42 km (ID: 49). (b) M_w 4.7, R_{epi}=15 km (ID: 259).

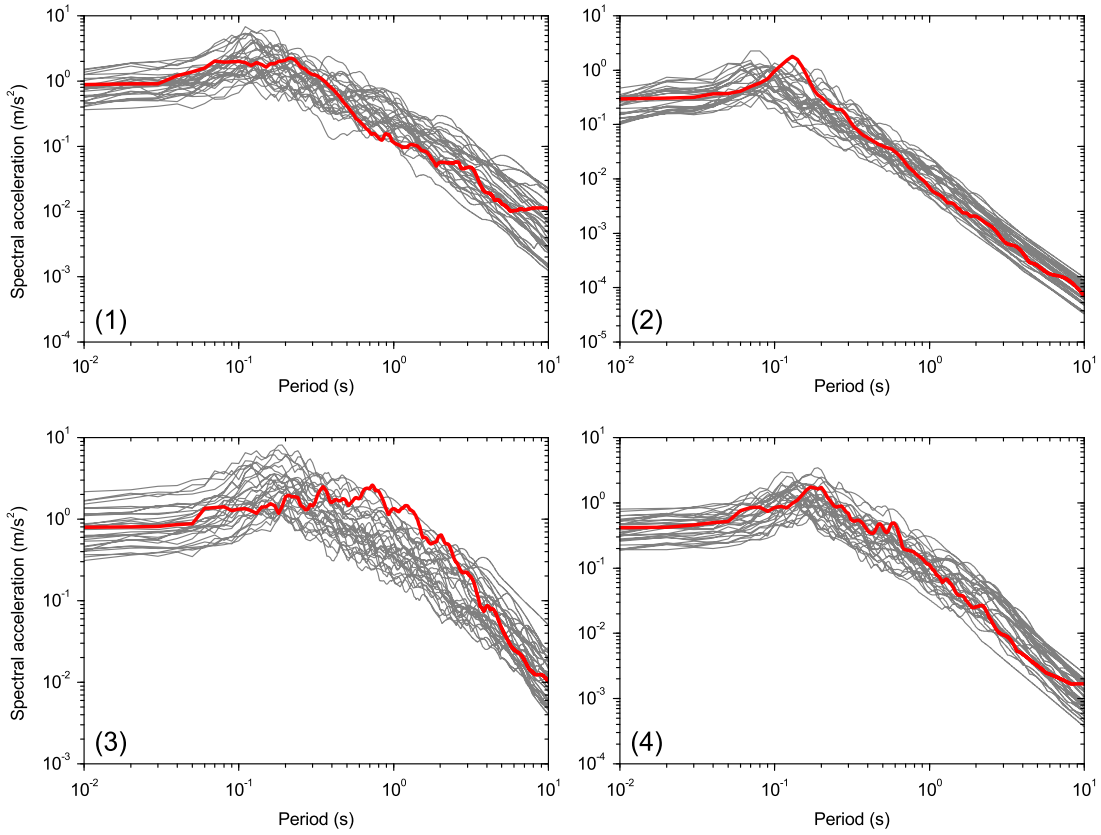

Fig. 14. 5% Damped acceleration response spectra for 30 simulations and real accelerograms (thick red line) for four real records (For interpretation of the references to color in this figure legend, the reader is referred to the web version of this article.).

4.3.1.5. Component of motion. Comparisons are made, either considering the larger horizontal (LH) component of motion, or the geometric mean (GM) of the two horizontal components of motion. Therefore, conversion factors between both types of components of motion are used. For this purpose, the coefficients proposed by Beyer and Bommer [83] are used. When making simulations with the proposed model, only the major component is used for LH comparisons and the geometric mean of the major and intermediate components $Sa_{GMxy}(T_i) = \sqrt{Sa_x(T_i) \cdot Sa_y(T_i)}$ [83] is used for GM comparisons.

Finally, two earthquake magnitudes are analysed throughout the following sections: (i) an earthquake M_w 6, that represents a "severe" event and (ii) an earthquake M_w 5, that represents a "moderate" event. The earthquake magnitude M_w 6 is selected as it is in line with the maximum magnitudes M_L 6.5–6.6 to be used in hazard analyses in the UK when considering a 10,000 years return period event [35] (an earthquake M_w 6 can be equivalent to an earthquake M_L 6.6 if the quadratic transformation formula of Johnston [49] is used). The choice of an earthquake M_w 5 as representative of a "moderate" event is made arbitrarily.

4.3.2. Peak ground acceleration estimation

Initially the effect of the number of simulations on the PGA estimation is studied. From this analysis, it was possible to conclude that the median PGA estimated with the proposed model tends to be reasonably stable when the number of simulations is equal or greater than 100. Differences when using more than 100 simulations can be considered negligible for structural engineering purposes. When 100 simulations are used several times to estimate the median PGA, there are slight differences in the final value as the accelerograms are stochastic in nature. Those differences, however, are numerically negligible. Consequently, analyses presented in the following sections are carried out considering the median of 100 simulations using the model proposed. Fig. 15 shows PGA estimation for earthquake magnitudes M_w 5 and 6, considering epicentral distances between 10 and 100 km for the UK (rock conditions), Europe and the Middle East (rock conditions) and SCRs (hard rock conditions). The standard deviation is shown for the results obtained with the proposed model and for one GMPE selected arbitrarily as the one that showed the closest behaviour to the proposed model for each group, namely, Rietbrock et al. [37] for the UK, Akkar et al. [72] for Europe and the Middle East, and Chen [79] for SCRs. Additionally, Table 9 provides a numerical summary of the data depicted in Fig. 15.

It is worth mentioning that the reason for taking the upper bound limit for epicentral distances as 100 km is due to the limitation of the proposed model to properly predict the rate of PGA attenuation for such distances. In other words, for epicentral distances longer than 100 km, the model tends to predict similar PGAs predicted for 90–100 km distance. This limitation of the model is due to the lack of information in the dataset (high epistemic uncertainty) of accelerograms recorded for epicentral distances longer than 100 km (see Fig. 2 for confirmation). Nevertheless, for structural engineering purposes, this limitation is relatively irrelevant: examples of disaggregation of hazard curves for the UK for a 10,000-years-return-period event [20,35,54], showed that earthquake distances longer than 100 km are of little or no significance in seismic hazard. Consequently, the upper bound of 100 km is considered sufficient for the purposes of risk analyses in the UK.

4.3.2.1. PGA estimation for the UK. GMPEs 1, 2, 3 and 4 in Table 8 are used for comparisons in the UK for the larger horizontal component of motion and consider generic rock conditions. GMPEs 1 and 2 are relevant in the UK as they have been extensively used for seismic hazard assessments of high-risk civil

Table 8
GMPEs selected for comparisons with the model proposed in this work.

N	Reference	Specific region	GMP[a]	HC[b]	M[c]	R[d]	Site classification	Style of faulting
	United Kingdom							
1	PML (1982) [68]	UK	PGA, PSV	LH	M_s	R_h	Rock, stiff soil and soft soil	Not included
2	PML (1985) [69]	UK	PGA, PSV	LH	M_s	R_h	Rock, stiff soil and soft soil	Not included
3	Musson et al. (1994) [70]	UK	PGA, PSV	LH	M_L	R_h	Not included	Not included
4	Rietbrock et al. (2013) [37]	UK	PGA, PGV, PSA	GM	M_w	R_{JB}	Hard rock (V_{s30}∼2300 m/s)	Not included
	Europe							
5	Akkar and Bommer (2010) [56]	Europe, Mediterranean Region and the Middle East	PGA, PGV, PSA	GM	M_w	R_{JB}	Rock ($V_{s30}>750$ m/s), Stiff soil ($360<V_{s30}<750$ m/s) Soft soil ($V_{s30}<360$ m/s)	Normal, strike-slip and reverse
6	Ambraseys et al. (2005) [50]	Europe and the Middle East	PGA, Sa	LH	M_w	R_{JB}	Rock ($V_{s30}>750$ m/s), Stiff soil ($360<V_{s30}<750$ m/s) Soft soil ($180<V_{s30}<360$ m/s) Very soft soil ($V_{s30}<180$ m/s)	Normal, strike-slip, thrust (reverse) and odd
7	Bommer et al. (2007) [71]	Europe and the Middle East	PGA, PSA	GM	M_w	R_{JB}	Rock ($V_{s30}>750$ m/s), Stiff soil ($360<V_{s30}<750$ m/s) Soft soil ($V_{s30}<360$ m/s)	Normal, strike-slip and reverse
8	Akkar et al. (2014) [72]	Europe and the Middle East	PGA, PSA	GM	M_w	R_{JB}, R_{ep}, R_{hyp}	Direct specification of V_{s30} (reference $V_{s30}=750$ m/s)	Normal, strike-slip and reverse
9	Dahle et al. (1990) [73]	Intraplate regions	PGA, PSV	LH	M_s	R_{hyp}	Not included	Not included
	Stable Continental Regions							
10	Toro et al. (1997) [74]	Central and Eastern North America	PGA, Sa	LH	M_w, m_{Lg}	R_{JB}	Hard rock (V_{s30}∼1800 m/s)	Not included
11	Campbell (2003) [75]	Eastern North America	PGA, PSA	GM	M_w	R_{rup}	Hard rock ($V_{s30}=2800$ m/s)	Not included
12	Liang et al. (2008) [76]	Australia	PGA, PGV, Sa	LH	M_L	R_{epi}	Generic rock	Not included
13	Kennedy et al. (2005) [77]	Australia	PGA,PGV	LH	M_L	R_{epi}	Generic rock	Not included
14	Raghu Kanth and Iyengar (2007) [78]	India	PGA, Sa	LH	M_w	R_{hyp}	Hard rock ($V_{s30}=3600$ m/s)	Not included
15	Chen (2008) [79]	Western China	PGA	LH, SH	M_L,M_s	R_{epi}	Not included	Not included

[a] Ground motion parameter predicted: PGA: peak ground acceleration; PGV, peak ground velocity; PSA: pseudospectral acceleration; PSV: pseudospectral velocity; Sa: spectral acceleration.
[b] Definition of the horizontal component: GM: geometric mean; LH: larger horizontal component; SH: smaller horizontal component.
[c] Magnitude scale used.
[d] Distance metric used.

structures. As mentioned by Lubkowski et al. [6], they have been used in the seismic risk assessment of "nuclear facilities, offshore oil and gas platforms, large dams, military installations and even the Channel Tunnel". Despite their widespread use, many concerns have been raised on the suitability of such predictive equations, calibrated about 30 years ago, and the necessity of upgrading earthquake estimation in the UK [34]. It is worth mentioning that the GMPEs 1, 2 and 3 were obtained indirectly through the comprehensive compilation of published GMPEs reported by Douglas [47]. GMPE 4 was the latest GMPE specifically calibrated for the UK found in the literature. This study calibrated two models based on the dependency/independency with magnitude of the stress parameter that defines the expected Fourier spectra of British earthquakes.

Fig. 15a shows that the PGAs estimated by the proposed model agree reasonably well with the magnitude-dependent stress parameter model reported by Rietbrock et al. [37]. In general, the models of PML [68–69] and Musson et al. [70] predicted higher values of PGAs, especially for epicentral distances shorter than 60–70 km. The constant stress parameter model of Rietbrock et al. [37] predicted systematically lower values of PGAs compared to the estimations made using the proposed model. The fact that the models of PML [68,69] estimated greater values of PGAs in the whole range of distances, compared to the proposed model, is a somewhat expected outcome. Such prediction equations were calibrated using datasets that comprised earthquakes from sites such as Central America, Greece, New Zealand and California. These zones belong to different tectonic regimes than those in Britain, and in general, they are more seismically active zones. This fact has raised many concerns on the validity of the PML equations and their current use in the British nuclear industry [34]. It is also likely that the use of PML equations may have led to an overestimation of seismic hazard analyses for nuclear sites in the UK.

4.3.2.2. PGA estimation for Europe and the Middle East. It is desirable to compare the proposed model with other models developed for the region of NW Europe. An early attempt was the model developed by Ambraseys [44] although the attenuation was modelled using the Medvedev–Sponheuer–Karnik (MSK) intensity scale. No PGA attenuation model is found in literature that has been calibrated with information exclusively taken from this region. Consequently, the closest models suitable for comparisons with the proposed model could be models calibrated using data from the wider region of Europe and the Middle East.

GMPEs 5, 6, 7, 8 and 9 in Table 8 are used for comparisons in Europe and the Middle East for the larger horizontal component of motion and consider generic rock conditions. GMPEs 5 to 7 are models widely and traditionally used in Europe; whereas GMPE 8 is part of the new generation of attenuation relations recently developed for Europe and the Middle East. This GMPE was randomly selected as representative from the five models that belong to the same project. Comprehensive comparisons among such five models can be found in Douglas et al. [57].

From Fig. 15b, it can be observed that the PGAs estimated by the proposed model, in general, fall below the predictions made by the selected GMPEs, especially for epicentral distances <60–

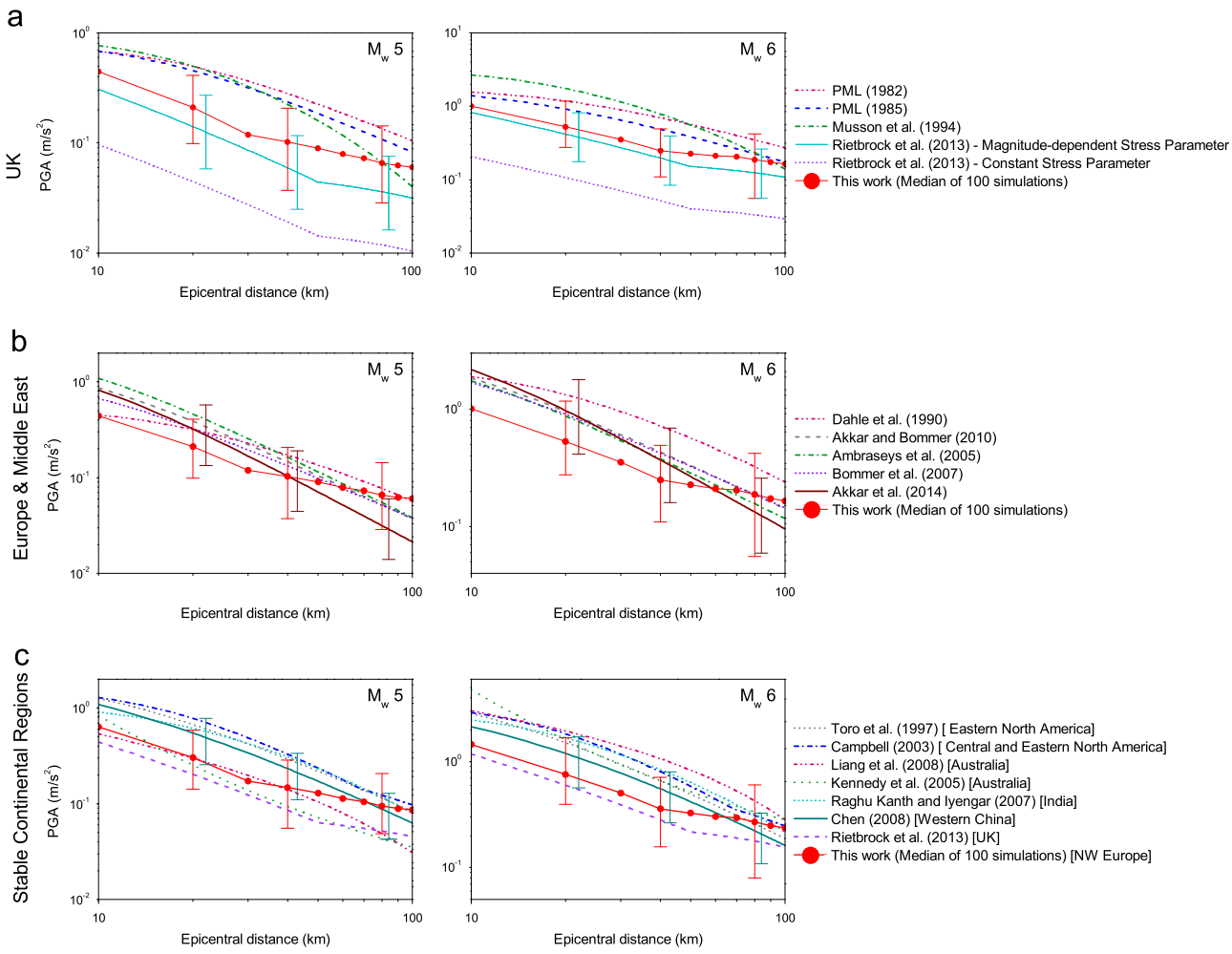

Fig. 15. PGA estimation for two earthquake magnitudes M_w 5 and 6, epicentral distances of 10 km $< R_{epi} <$ 100 km for (a) the UK in rock, (b) Europe and the Middle East in rock and (c) SCRs in hard rock. See text for details on adjustments.

70 km. For greater distances (up to 100 km), the predictions made by the two sets of models are in the same region. The proposed model, in general, tends to predict lower PGAs compared to GMPEs developed for Europe and intraplate regions, and this an expected outcome. The studies selected have broader target geographical regions, and therefore, they have been subjected to different and more active tectonic processes compared to NW Europe.

4.3.2.3. PGA estimation for SCRs. As discussed in Section 2, there is no total agreement as to what extent different SCRs can be considered equivalent in terms of their seismicity features. Johnston [36] defined nine major SCRs worldwide and this section focuses on five of them: Eastern North America (ENA), Australia, India, Western China and NW Europe.

The comparisons presented are for the geometric mean of the two horizontal components of motion and consider generic hard rock conditions. It is acknowledged that there is a high variability in the definition of hard rock made by the GMPEs selected (from V_{S30} = 1800 m/s made by Toro et al. [74] to V_{S30} = 3600 m/s made by Raghu Kanth and Iyengar [78]). Nevertheless, amplifications in such high range of velocities can be assumed negligible and comparisons can still be made in terms of generic site classes [37]. Even though the site classification of the Australian models reported by Liang et al. [76] and Kennedy et al. [77] is generic rock, it is unlikely that this coincides with the description of generic rock considered in this analysis. Rather, they seem to be more in agreement with generic hard rock conditions, as is suggested by the comparisons with ENA presented in Liang et al. [76]. Consequently, and for the sake of simplicity, both Australian models are not adjusted to generic hard rock conditions. For the model of Western China, developed by Chen [79], that does not include site classification, it is assumed that it was calibrated for generic hard rock conditions. Finally, the magnitude-dependent stress parameter model reported by Rietbrock et al. [37] is included in this analysis to observe differences in attenuation between the particular case of the UK and other SCRs.

Fig. 15c shows that there is a rather wide range of PGA intensities and attenuation rates among these SCRs. An explanation supporting this statement can be found in Johnston et al. [36]. All nine major SCRs share the same primary crustal features, but there are still differences between them as each continent has experienced its own particular geological/tectonic development. Nevertheless, from a broad point of view, it seems that ENA, Australia and India exhibit a rather similar behaviour; Western China can be considered to have an average behaviour whereas NW Europe has smaller intensities compared to other SCRs. These results are in reasonably good agreement with findings reported by Bakun and McGarr [84]. Although in their analysis the attenuation is modelled using the Modified Mercalli Intensity (MMI) scale, they suggested that ENA and NW Europe could be considered as the upper and lower limits of intensity

Table 9
Numerical summary for the PGA estimation shown in Fig. 15 (units in m/s^2).

Magnitude		M_w 5			M_w 6			σ[a]
R_{epi} (km)		20	40	80	20	40	80	
		United Kingdom						
1	PML (1982) [68]	0.496	0.281	0.135	1.176	0.698	0.347	0.543
2	PML (1985) [69]	0.454	0.237	0.108	0.919	0.486	0.226	0.49
3	Musson et al. (1994) [70]	0.499	0.225	0.067	1.742	0.784	0.232	0.65[b]
4	Rietbrock et al. (2013) [37] – Mod 1	0.045	0.019	0.012	0.107	0.052	0.033	0.436
5	Rietbrock et al. (2013) [37] – Mod 2	0.140	0.059	0.036	0.417	0.197	0.124	0.335
This work		**0.211**	**0.103**	**0.066**	**0.528**	**0.249**	**0.187**	**0.764–0.713**[c]
		Europe						
6	Akkar and Bommer (2010) [56]	0.387	0.146	0.052	0.956	0.432	0.186	0.279
7	Ambraseys et al. (2005) [50]	0.462	0.164	0.055	0.872	0.378	0.156	0.358–0.289
8	Bommer et al. (2007) [71]	0.325	0.133	0.051	0.903	0.421	0.187	0.352–0.286
9	Akkar et al. (2014) [72]	0.321	0.104	0.032	0.972	0.370	0.133	0.731
10	Dahle et al. (1990) [73]	0.317	0.172	0.077	1.327	0.721	0.322	0.83
This work		**0.211**	**0.103**	**0.066**	**0.528**	**0.249**	**0.187**	**0.764–0.713**[c]
		Stable Continental Regions						
11	Toro et al. (1997) [74]	0.672	0.293	0.115	1.511	0.659	0.258	0.65–0.71
12	Campbell (2003) [75]	0.779	0.329	0.123	1.834	0.805	0.310	0.69–0.59[c]
13	Liang et al. (2008) [76]	0.298	0.141	0.048	1.941	1.067	0.426	1.166
14	Kennedy et al. (2005) [77]	0.252	0.094	0.043	1.600	0.662	0.336	0.33
15	Raghu Kanth and Iyengar (2007) [78]	0.614	0.309	0.116	1.675	0.842	0.317	0.329
16	Chen (2008) [79]	0.548	0.233	0.088	1.193	0.555	0.222	0.240
17	Rietbrock et al. (2013) [37] – Mod 2	0.202	0.086	0.052	0.600	0.283	0.178	0.335
This work		**0.303**	**0.147**	**0.095**	**0.760**	**0.358**	**0.270**	**0.751–0.701**[c]

[a] Standard deviation in log units. Some models reported single values for σ (magnitude independent). Models that reported magnitude-dependent values for σ are shown for the two magnitudes selected for this comparison.
[b] It is a recommended value although not calculated in regression.
[c] Standard deviation is both magnitude- and distance-dependent. Values shown are the average for the three distances selected for this comparison.

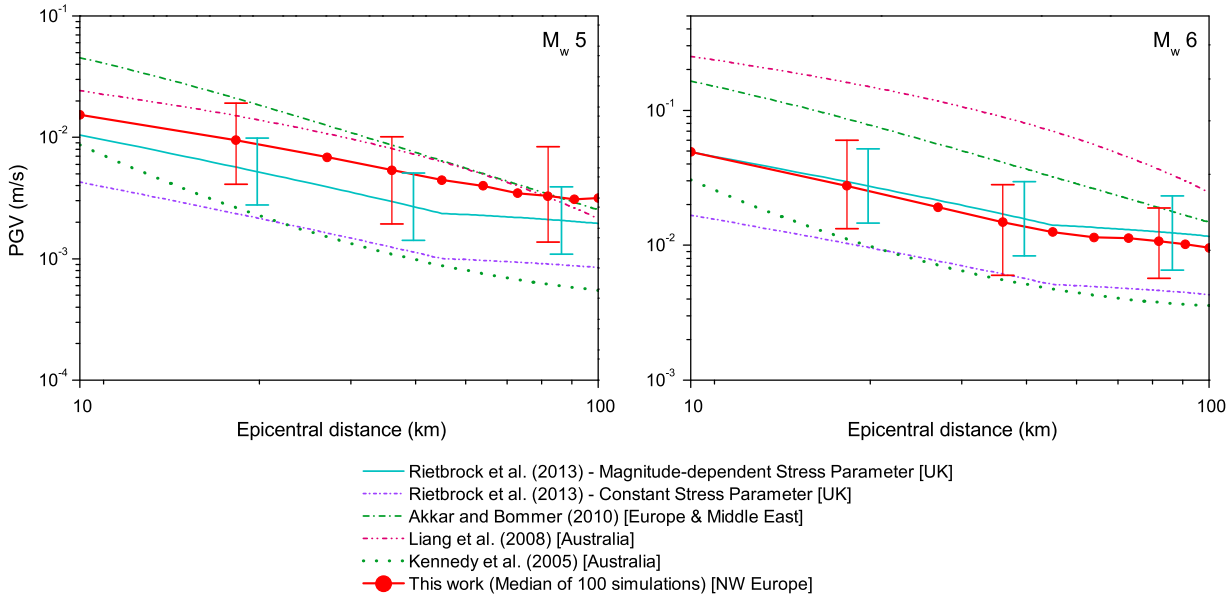

Fig. 16. PGV estimation for two earthquake magnitudes M_w 5 and 6, epicentral distances of 10 km < R_{epi} < 100 km for the UK, Europe and the Middle East and some SCRs in hard rock. See text for details on adjustments.

attenuation among SCRs, and the rest (a common SCR) might be somewhere in between.

4.3.3. *Peak ground velocity estimation*

PGV estimation was made considering the few GMPEs that reported it, i.e. GMPEs 4, 5, 12 and 13 in Table 8; consequently, comparisons were not possible to make using the same geographic categories as for the PGA. Fig. 16 shows the PGV estimation for the geometric mean of two horizontal components for earthquake magnitudes M_w 5 and 6, considering epicentral distances between 10 and 100 km in hard rock conditions for the UK, Europe and the Middle East, and SCRs. These predictions are compared to the median PGV of 100 simulations made with the proposed model using a corner frequency of $\omega_c = \pi$ (rad/s)in all simulated accelerograms. The standard deviation is shown for the results obtained with the proposed model and for one GMPE selected arbitrarily as the one that showed the closest behaviour to the proposed model, namely, Rietbrock et al. [37]. Additionally, Table 10 provides a numerical summary of the data depicted in Fig. 16.

Table 10
Numerical summary for the PGV estimation shown in Fig. 16 (units in m/s).

Magnitude		M_w 5			M_w 6			σ
R_{epi} (km)		20	40	80	20	40	80	
1	Rietbrock et al. (2013) [37] – Mod 1	2.35E-3	1.24E-3	9.05E-4	1.03E-2	6.12E-3	4.62E-3	0.347
2	Rietbrock et al. (2013) [37] – Mod 2	5.69E-3	2.95E-3	2.11E-3	2.95E-2	1.70E-2	1.26E-2	0.276
3	Akkar and Bommer (2010) [56]	2.10E-2	8.62E-3	3.42E-3	8.63E-2	4.11E-2	1.90E-2	0.278
4	Liang et al. (2008) [76]	1.51E-2	8.08E-3	3.21E-3	1.61E-1	8.91E-2	3.65E-2	1.3
5	Kennedy et al. (2005) [77]	2.63E-3	1.09E-3	6.18E-4	1.11E-2	5.54E-3	3.77E-3	0.423
This work		**9.46E-3**	**5.41E-3**	**3.30E-3**	**2.75E-2**	**1.48E-2**	**1.15E-2**	**0.336–0.373**[a]

[a] Standard deviation is both magnitude- and distance-dependent. Values shown are the average for the three distances selected for the corresponding magnitudes used in this comparison.

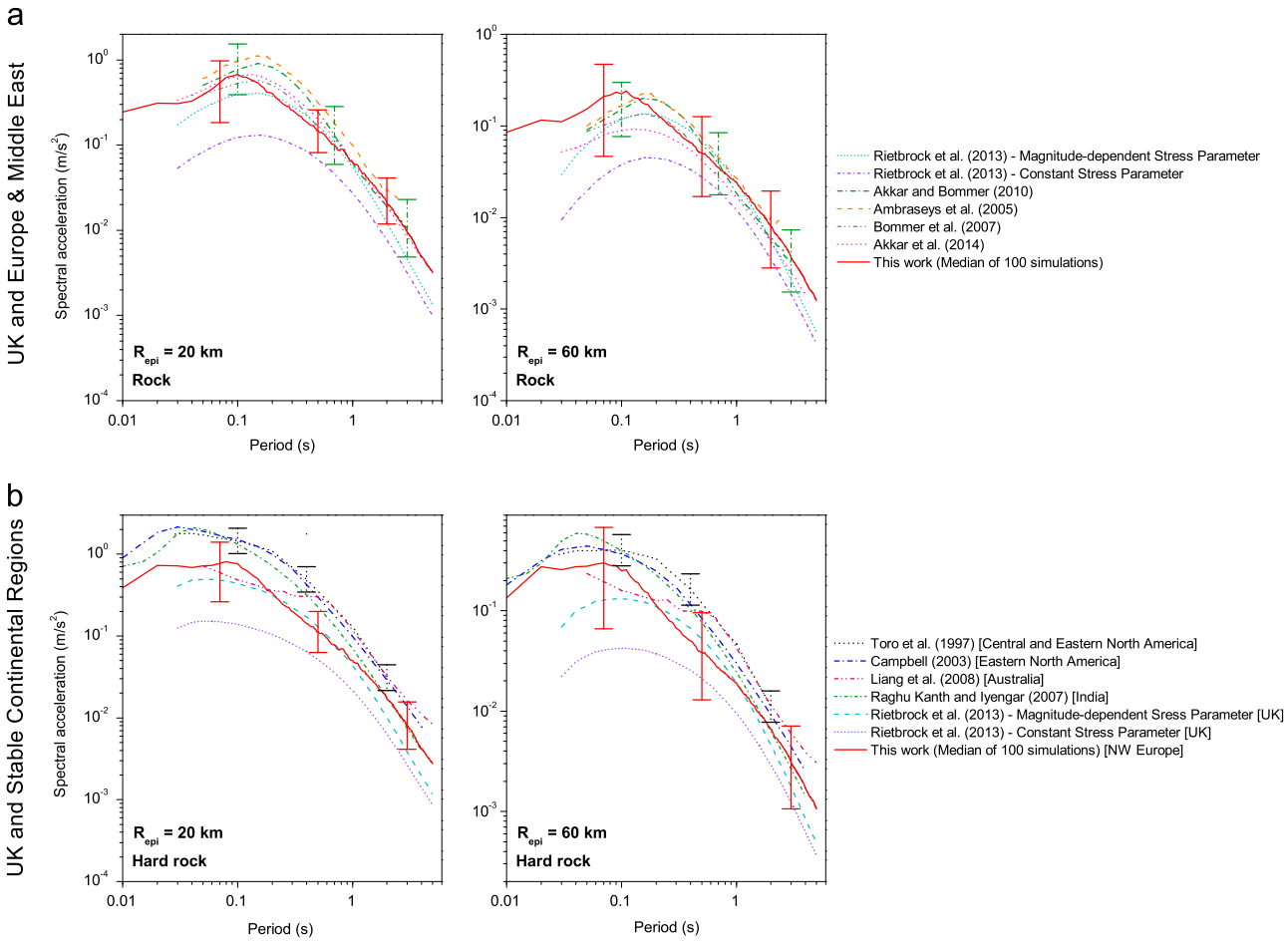

Fig. 17. Spectral acceleration estimation for an earthquake magnitude M_w 5, R_{epi}=20 and 60 for (a) UK and Europe and the Middle East in rock; (b) UK and SCRs in hard rock. See text for details on adjustments.

Fig. 16 shows that the PGVs estimated by the proposed model agree reasonably well with the magnitude-dependent stress parameter model reported by Rietbrock et al. [37]. In general, the European model of Akkar and Bommer [56] and the Australian model of Liang et al. [76] predicted higher values of PGVs in the whole range of distances. The constant stress parameter model of Rietbrock et al. [37] and the Australian model of Kennedy et al. [77] predicted systematically lower values of PGVs compared to the estimations made with the proposed model. This overall behaviour is similar to what was obtained for PGA estimations.

4.3.4. Spectral acceleration estimation

As the two models developed by Rietbrock et al. [37] are the only models found in literature that predict spectral accelerations calibrated exclusively for the UK, the comparisons presented in this section are simultaneously made for UK-Europe and the Middle East, and UK-SCRs, both in terms of the geometric mean of two horizontal components. Figs. 17 and 18 show the acceleration response spectra for earthquake magnitudes M_w 5 and 6 with two different epicentral distances, R_{epi}=20 and 60 km for UK/Europe & the Middle East (rock conditions) and UK/SCRs (hard rock conditions). These predictions are compared to the median spectrum of 100 simulations made with the proposed model using a corner frequency of $\omega_c = \pi$ (rad/s)in all simulated accelerograms. The standard deviation is shown for the results obtained with the proposed model and for one GMPE selected arbitrarily as the one that showed the closest behaviour to the proposed model for each group, namely, Akkar and Bommer [56] for Europe and Toro et al.

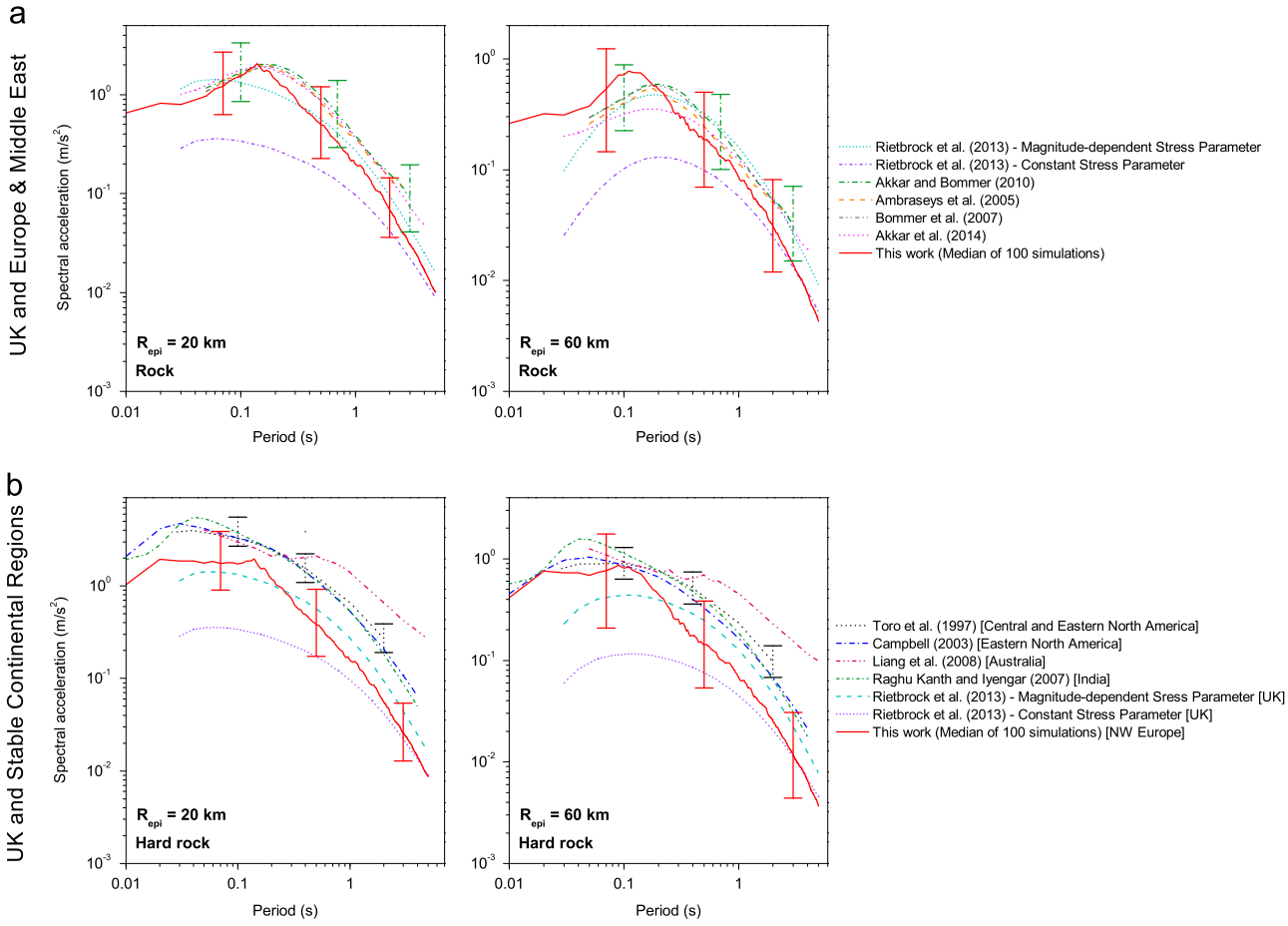

Fig. 18. Spectral acceleration estimation for an earthquake magnitude M_w 6, R_{epi}=20 and 60 for (a) UK and Europe and the Middle East in rock; (b) UK and SCRs in hard rock. See text for details on adjustments.

Table 11
Numerical summary for the spectral acceleration estimation shown in Fig. 17 (units in m/s^2).

R_{epi} (km)		20–60			σ		
Period (s)		**0.1**	**0.5**	1	**0.1**	**0.5**	1
		UK and Europe					
1	Rietbrock et al. (2013) [37] – Mod 1	0.123–0.038	0.067–0.028	0.027–0.012	0.428	0.378	0.350
2	Rietbrock et al. (2013) [37] – Mod 2	0.393–0.118	0.169–0.069	0.055–0.024	0.325	0.282	0.268
3	Akkar and Bommer (2010) [56]	0.777–0.151	0.244–0.064	0.062–0.018	0.297	0.329	0.325
4	Ambraseys et al. (2005) [50]	0.965–0.164	0.313–0.075	0.099–0.027	0.392	0.422	0.323
5	Bommer et al. (2007) [71]	0.534–0.119	0.161–0.047	–	0.381	0.388	–
6	Akkar et al. (2014) [72]	0.645–0.088	0.202–0.042	0.065–0.017	0.802	0.788	0.798
This work		**0.676–0.223**	**0.147–0.051**	**0.064–0.024**	**0.463**	**0.573**	**0.660**
		UK and Stable Continental Regions					
7	Rietbrock et al. (2013) [37] – Mod 1	0.139–0.042	0.052–0.021	0.022–0.009	0.428	0.378	0.350
8	Rietbrock et al. (2013) [37] – Mod 2	0.442–0.133	0.130–0.053	0.043–0.019	0.325	0.282	0.268
9	Toro et al. (1997) [74]	1.454–0.401	0.493–0.164[a]	0.130–0.046	0.66	0.69	0.70
10	Campbell (2003) [75]	1.497–0.368	0.300–0.084	0.099–0.030	0.715	0.683	0.661
11	Liang et al. (2008) [76]	0.489–0.160	0.301–0.099	0.118–0.043	–	–	–
12	Raghu Kanth and Iyengar (2007) [78]	1.321–0.398	0.228–0.077	0.070–0.024	0.285	0.247	0.222
This work		**0.761–0.251**	**0.112–0.039**	**0.050–0.019**	**0.455**	**0.563**	**0.649**

[a] Results shown are for a structural period of 0.4 s.

[74] for SCRs. Additionally, Tables 11 and 12 provide a numerical summary of the data depicted in Figs. 17 and 18.

Fig. 17 shows that the predictions for an earthquake magnitude M_w 5 made with the proposed model tend to be in between those from the magnitude-dependent stress parameter model of Rietbrock et al. [37] and the other models calibrated for Europe and the Middle East, and SCRs for the whole range of structural periods in the epicentral distances considered. Fig. 18 shows that for an earthquake magnitude M_w 6, for shorter periods, say 0.05 to 0.2 s, the predictions made with the proposed model tend to be in relatively close agreement with other models calibrated for Europe and the Middle East, and SCRs. However, for longer periods, say 0.5 to 5 s, the predictions made with the proposed model are mostly in between the two UK models developed by Rietbrock et al. [37].

Table 12
Numerical summary for the spectral acceleration estimation shown in Fig. 18 (units in m/s^2).

R_{epi} (km)		20–60			σ		
Period (s)		**0.1**	**0.5**	1	**0.1**	**0.5**	1
		UK and Europe					
1	Rietbrock et al. (2013) [37] – Mod 1	0.301–0.102	0.224–0.099	0.122–0.057	0.428	0.378	0.350
2	Rietbrock et al. (2013) [37] – Mod 2	1.181–0.392	0.741–0.322	0.344–0.160	0.325	0.282	0.268
3	Akkar and Bommer (2010) [56]	1.687–0.447	0.980–0.305	0.382–0.132	0.297	0.329	0.325
4	Ambraseys et al. (2005) [50]	1.608–0.397	0.820–0.246	0.364–0.113	0.313	0.340	0.328
5	Bommer et al. (2007) [71]	1.575–0.44	0.867–0.279	–	0.308	0.363	–
6	Akkar et al. (2014) [72]	1.781–0.317	0.883–0.239	0.368–0.123	0.802	0.788	0.798
This work		**1.543–0.720**	**0.493–0.187**	**0.199–0.086**	**0.935**	**0.811**	**0.755**
		UK and Stable Continental Regions					
7	Rietbrock et al. (2013) [37] – Mod 1	0.338–0.115	0.171–0.076	0.097–0.045	0.428	0.378	0.350
8	Rietbrock et al. (2013) [37] – Mod 2	1.329–0.441	0.566–0.247	0.272–0.126	0.325	0.282	0.268
9	Toro et al. (1997) [74]	3.268–0.902	1.556–0.517[a]	0.657–0.233	0.709	0.735	0.753
10	Campbell (2003) [75]	3.293–0.857	1.142–0.330	0.533–0.166	0.625	0.597	0.593
11	Liang et al. (2008) [76]	2.894–0.935	2.115–0.694	1.402–0.457	–	–	–
12	Raghu Kanth and Iyengar (2007) [78]	3.744–1.127	1.176–0.396	0.533–0.185	0.285	0.247	0.222
This work		**1.737–0.811**	**0.377–0.143**	**0.157–0.068**	**0.920**	**0.797**	**0.742**

[a] Results shown are for a structural period of 0.4 s.

5. Discussion

On the definition of NW Europe: Though different definitions of NW Europe have been used in the literature, it is acknowledged that the F–E regionalisation scheme [45] is only intended to set clear boundaries among different regions of the Earth and not necessarily based on their tectonic features. However, the NW European area defined by the F–E scheme is contained within the borders of the European SCR defined by Johnston [36]; hence, a relatively similar tectonic behaviour may be expected within this constrained area. It may be argued that the F–E definition of NW Europe includes areas of high seismic activity (in relative terms), such as the Alps and the Pyrenees. However, this was deemed suitable as it was necessary to include areas that possessed recorded accelerograms from strong earthquake magnitudes, say M_w 6–6.5. In this light, the model proposed would be calibrated using data from strong earthquakes (for NW European standards) that were recorded in areas that could be assumed to be comparable due to geographical proximity. This would avoid the use of accelerograms from such high earthquake magnitudes recorded in areas that possess more available information (e.g. active crustal regions) but whose characteristics may not be directly applied in NW Europe, as discussed in Section 2.

Underlying assumption of the model proposed: The database of British earthquakes is mainly composed of small magnitude events whose features are unsuitable for predicting the characteristics of moderate-to-large earthquake accelerograms. For this reason, it is assumed that the inherent features of accelerograms (intensity, frequency content and time duration), caused by moderate-to-strong earthquakes in Britain, would be similar to those in the Stable Continental Region to which the UK belongs, namely NW Europe. In terms of PGA, estimations made with the proposed model closely follow predictions made with the latest GMPEs calibrated for the UK in the range of magnitudes and distances of interest in probabilistic seismic hazard analysis in Britain. Also, estimations made with the proposed model confirm a result that has been earlier reported in the literature: i.e. NW Europe has associated smaller PGA intensities than other SCRs covered in earthquake engineering research. When compared with GMPEs calibrated for the wider region of Europe, it is expected that lower PGA estimations are obtained with the proposed model, as the European region comprises more seismically active zones than NW Europe. In general, this result is confirmed from the validation analyses performed.

Comparison with a NGA model: The stochastic accelerogram model reported by Rezaeian and Der Kiureghian [1,2] calibrated using a subset of the NGA database is used for a general comparison with the proposed model. Table 13 shows a detailed comparison in terms of the dataset, mathematical formulation, variable selection and marginal distributions, and regression analysis between the two models. Although both share the same mathematical model, Table 13 shows several differences between their developments. The various modifications introduced in this work were necessary to adopt in order to define a suitable model for NW European accelerograms' features.

Limitations: One of the limitations of the model proposed that could be envisaged *a priori* is related to the lack of information of the dataset for accelerograms recorded at epicentral distances longer than 100 km. As stated in Section 4.3, the model proposed was not able to appropriately capture the attenuation rate of PGAs, PGVs and spectral accelerations when simulating seismic scenarios for such distances. For this reason, in this article the applicability of the model was set to a maximum epicentral distance of 100 km. In this light, it is acknowledged that the model presented in this work possesses a rather high epistemic uncertainty. The epistemic uncertainty of this model can only be reduced by adding more accelerograms to the dataset; therefore, the model should be subjected to revisions/updates when more data are available.

GMPEs vs stochastic accelerogram models: As GMPEs do not primarily aim to provide ground motion accelerograms, nonlinear time-history analysis in the context of SPRA, could not rationally be performed based solely on such predictive models. For seismic assessment of critical structures, such as nuclear power stations, comprehensive sets of accelerograms compatible with the local seismicity are required. In this sense, the main objective of the model proposed is to establish a mathematical model able to simulate any number of accelerograms for any seismic scenarios (magnitude, distance, type of soil) within NW Europe. However, as GMPEs are widely used and recognised by practitioners/researchers, they can also be used as a validation framework of the model presented in this work.

6. Conclusions

A fully non-stationary stochastic ground motion accelerogram model for use in the NW European areas is developed, based on the

Table 13
Comparison between an NGA accelerogram model and this work.

	Rezaeian and Der Kiureghian [1,2]	**This work**
Target geographical region	Active crustal regions	Northwest Europe
Dataset		
Database	NGA	ISESD
Number of accelerograms	203	220
Magnitudes (M_w)	6.1–7.7	4–6.5
Distances	$10 < R_{rup} < 100$ km	$10 < R_{epi} < 100$ km
Type of soil	$V_{s30} > 600$ m/s	Rock, stiff and soft soil
Style of faulting	Strike-slip, reverse	Not included
Mathematical formulation		
Mathematical model	Rezaeian and Der Kiureghian [2]	Rezaeian and Der Kiureghian [2]
Time-modulating function	Gamma type (3 parameters)	Piece-wise type (6 parameters)
Linear filter	PSA SDOF (3 parameters)	PSA SDOF (3 parameters)
Total variables to simulate accelerograms	6	9
Variable selection		
Time-modulating function	1. Arias intensity, $\boldsymbol{I_a}$ 2. Effective duration, $\boldsymbol{D_{5-95}}$ 3. Middle time of the strong-shaking phase, $\boldsymbol{t_{mid}}$	1. Maximum intensity, α_1 2, 3. Controllers of decaying intensity, α_2, α_3 4. Start time, $\boldsymbol{T_0}$ 5, 6. Start and end time of strong-shaking phase, $\boldsymbol{T_1}$, $\boldsymbol{T_2}$
Filter parameter	1. Frequency at t_{mid}, $\omega_{\boldsymbol{mid}}$ 2. Rate of frequency change, ω' 3. Damping ratio, $\xi_{\boldsymbol{f}}$	1. Frequency at beginning, $\omega_{\boldsymbol{0}}$ 2. Frequency at end, $\omega_{\boldsymbol{f}}$ 3. Damping ratio, $\xi_{\boldsymbol{f}}$
Matching procedure for parameters of dataset's accelerograms	Nonlinear optimisation	Monte Carlo simulation
Marginal distributions of variables		
Time-modulating function	$\boldsymbol{I_a}$: Normal $\boldsymbol{D_{5-95}}$: Beta $\boldsymbol{t_{mid}}$: Beta	α_1, α_2, α_3: Generalised extreme value (GEV) $\boldsymbol{T_0}$: Lognormal $\boldsymbol{T_1}$, $\boldsymbol{T_0}$: Birnbaum–Saunders
Filter parameter	$\omega_{\boldsymbol{mid}}$: Gamma ω': Two-sided exponential $\xi_{\boldsymbol{f}}$: Beta	$\omega_{\boldsymbol{0}}$: Gamma $\omega_{\boldsymbol{f}}$: GEV $\xi_{\boldsymbol{f}}$: GEV
Regression analysis		
Modelling of random-effects regression	Rezaeian and Der Kiureghian's [1] algorithm	Abrahamson and Youngs's [67] algorithm
Type of functional form	Linear	Nonlinear
Functional form	$\nu_i = \beta_{i,0} + \beta_{i,1} \cdot F + \beta_{i,2} \cdot (M/7) + \beta_{i,3} \cdot (R/25) + \beta_{i,4} \cdot (V_{s30}/750)$ $i = 2, \ldots, 6$	$\nu_i = \beta_{i,0} + \beta_{i,1} \cdot M + \beta_{i,2} \cdot \sqrt{R} + \beta_{i,3} \cdot \ln(M \cdot R) + \beta_{i,4} \cdot D_1 + \beta_{i,5} \cdot D_2$ $i = 1, \ldots, 9$
Explanatory variables of functional form	$\boldsymbol{F}$=type of faulting $\boldsymbol{M}$=moment magnitude $\boldsymbol{R}$=distance-to-site $\boldsymbol{V_{s30}}$=shear-wave velocity (type of soil is modelled **quantitatively**)	$\boldsymbol{M}$=moment magnitude $\boldsymbol{R}$=epicentral distance $\boldsymbol{D_1}$ and $\boldsymbol{D_2}$=dummy variables (type of soil is modelled **qualitatively**)

time-modulated filtered white noise process proposed by Rezaeian and Der Kiureghian [1,2]. A functional form of predictive equations for such a process is presented which in turn is calibrated using a subset of the European database composed of 220 accelerograms recorded in NW Europe. This model simulates accelerograms compatible with seismic scenarios defined by earthquake magnitudes $4 < M_w < 6.5$, distance-to-site $10 \text{ km} < R_{epi} < 100$ km and different types of soil (rock, stiff and soft soil). The calibration of the predictive equations was performed by means of regression analysis. The statistical significance of the regressors proposed are considered appropriate to simulate accelerograms as it has been seen that the model is able to capture the natural variability of accelerograms for a specified seismic scenario. The conclusions from this research are summarised as follows:

* The definition of the boundaries for a NW European region that possesses uniform tectonic behaviour, which in turn could be considered representative for UK standards, seems to be a matter open to discussion as different definitions were found in the literature. The approach used in this work, based on the Flinn–Engdhal regionalisation scheme, was initially found to be a reasonable alternative to define an area of moderate-to-low seismic activity. This area includes recorded accelerogram data from earthquakes of magnitudes and distances relevant for structural engineering purposes.
* The predictive equations calibrated by means of the random-effects regression technique are able to account for the sample-dependency of the dataset used. Several functional forms for these predictive equations were tested. For simplicity, only one functional form, with the least possible number of explanatory variables, was chosen for all parameters that govern the stochastic process. This implies that different levels of statistical significance for the predictive equations were obtained. However, all predictive equations proposed were appropriate for explaining the statistical behaviour of the dependent variables at the standard 5% significance level normally used in statistical hypothesis testing.
* The model proposed requires three input variables typically used in structural engineering applications, namely, earthquake magnitude, distance-to-site and type of soil for a design seismic scenario. Once this information is set, the simulation of accelerograms is entirely made in the time domain and essentially involves the generation of random variables. In this light, this model is considered to be straightforward to define seismic inputs for nonlinear time-history analysis of structures.

* The predictive model proposed in this work was found to capture the natural variability of accelerograms produced by different seismic scenarios. Verifications using recorded accelerograms from NW Europe show that a real recording can be considered to be one accelerogram likely to be produced by a specific seismic scenario. The artificial recordings are able to simulate the natural dispersion associated to the earthquake generation phenomenon.
* Regarding PGA estimations obtained with the model proposed, it is found that there is a reasonably good agreement with the latest predictive models calibrated for the UK and Europe, for the magnitudes and distances of interest in seismic hazard and risk analysis. However, when compared with the models used in hazard assessments in the UK [68,69], the proposed model systematically estimates lower PGAs. This may support some concerns reported in the literature on the validity of such equations, especially for their use in the British nuclear industry. Even though further evidence is required to support this statement, it is likely that such models may have led to conservative results for nuclear sites in the UK. Additionally, comparisons made with other SCRs show that PGA intensities and attenuation rates are somewhat different. This may be explained by the fact that each SCR has experienced its own tectonic evolution. Nevertheless, results obtained in this work suggest that Eastern North America, Australia and India possess a rather similar behaviour and have associated higher PGA intensities. On the other hand, NW Europe can be considered to have associated smaller PGA intensities. Finally, Western China could be regarded as possessing an average behaviour.
* Regarding estimations on spectral acceleration, there is also a reasonably good agreement between the model proposed and predictive models calibrated for the UK, Europe and other SCRs. This is valid for a wide range of periods for the magnitudes and distances of interest for time-history analyses of structures. Consequently, it can be concluded that the proposed model is suitable to rationally define the loading input in structural engineering analyses for the NW European regions.

Acknowledgments

The authors would like to thank Dr Brian Ellis, Ellis Consultant, for his constructive comments on the manuscript.

References

[1] Rezaeian S, Der Kiureghian A. Simulation of synthetic ground motions for specified earthquake and site characteristics. Earthq Eng Struct Dyn 2010;39:1155–80.
[2] Rezaeian S, Der Kiureghian A. A stochastic ground motion model with separable temporal and spectral nonstationarities. Earthq Eng Struct Dyn 2008;37:1565–84.
[3] McGuire RK. Seismic hazard and risk analysis. Oakland, California, USA: Earthquake Engineering Research Institute; 2004.
[4] Huang Y-N, Whittaker AS, Luco N. A probabilistic seismic risk assessment procedure for nuclear power plants: (I) Methodology. Nucl Eng Des 2011;241:3996–4003.
[5] Huang Y-N, Whittaker A, Luco N. A probabilistic seismic risk assessment procedure for nuclear power plants: (II) Application. Nucl Eng Des 2011;241:3985–95.
[6] Lubkowski Z, Bommer JJ, Baptie B, Bird J, Douglas J, Free M, Hancock J, Sargeant S, Sartain N, Strasser F. An evaluation of attenuation relationships for seismic hazard assessment in the UK. In: Proceedings of the 13th World conference on earthquake engineering. Vancouver (Canada); 2004. p. 1422.
[7] Musson RMW. UK seismic hazard assessments for strategic facilities: a short history. In: Proceedings of the 30th national GNGTS conference (Gruppo Nazionale di Geofisica della Terra Solida). Trieste (Italy); 2011.
[8] Katsanos EI, Sextos AG, Manolis GD. Selection of earthquake ground motion records: a state-of-the-art review from a structural engineering perspective. Soil Dyn Earthq Eng 2010;30:157–69.
[9] NIST. Selecting and scaling earthquake ground motions for performing response-history analyses. Gaithersburg, Maryland, USA: National Institute of Standards and Technology (NIST); 2012.
[10] Huang Y-N, Whittaker A, Luco N, Hamburger. Scaling earthquake ground motions for performance-based assessment of buildings. J Struct Eng 2011;137:311–21.
[11] Luco N, Bazzurro P. Does amplitude scaling of ground motion records result in biased nonlinear structural drift responses? Earthq Eng Struct Dyn 2007;36:1813–35.
[12] Grant DN, Diaferia R. Assessing adequacy of spectrum-matched ground motions for response history analysis. Earthq Eng Struct Dyn 2013;42:1265–80.
[13] Hancock J, Bommer JJ, Stafford PJ. Numbers of scaled and matched accelerograms required for inelastic dynamic analyses. Earthq Eng Struct Dyn 2008;37:1585–607.
[14] Ay BÖ, Akkar S. A procedure on ground motion selection and scaling for nonlinear response of simple structural systems. Earthq Eng Struct Dyn 2012;41:1693–707.
[15] Baker JW. Conditional mean spectrum: tool for ground-motion selection. J Struct Eng 2011;137:322–31.
[16] Watson-Lamprey J, Abrahamson N. Selection of ground motion time series and limits on scaling. Soil Dyn Earthq Eng 2006;26:477–82.
[17] Bozorgnia Y, Abrahamson NA, Atik LA, Ancheta TD, Atkinson GM, Baker JW, Baltay A, Boore DM, Campbell KW, Chiou BSJ, Darragh R, Day S, Donahue J, Graves RW, Gregor N, Hanks T, Idriss IM, Kamai R, Kishida T, Kottke A, Mahin SA, Rezaeian S, Rowshandel B, Seyhan E, Shahi S, Shantz T, Silva W, Spudich P, Stewart JP, Watson-Lamprey J, Wooddell K, Youngs R. NGA-West2 research project. Earthq Spectra 2014;30:973–87.
[18] Douglas J. Preface of special issue: a new generation of ground-motion models for Europe and the Middle East. Bull Earthq Eng 2014;12:307–10.
[19] Atkinson GM. Integrating advances in ground-motion and seismic-hazard analysis. In: Proceedings of the 15th World conference on earthquake engineering. Lisbon (Portugal); 2012.
[20] Musson RMW. The use of Monte Carlo simulations for seismic hazard assessment in the U.K.; 2000.
[21] Assatourians K, Atkinson GM. EqHaz: an open-source probabilistic seismic-hazard code based on the Monte Carlo Simulation Approach. Seism Res Lett 2013;84:516–24.
[22] Weatherill G, Burton PW. An alternative approach to probabilistic seismic hazard analysis in the Aegean region using Monte Carlo simulation. Tectonophysics 2010;492:253–78.
[23] Douglas J, Aochi H. A survey of techniques for predicting earthquake ground motions for engineering purposes. Surv Geophys 2008;29:187–220.
[24] Halldórsson B, Mavroeidis G, Papageorgiou A. Near-fault and far-field strong ground-motion simulation for earthquake engineering applications using the specific barrier model. J Struct Eng 2011;137:433–44.
[25] Liu P, Archuleta RJ, Hartzell SH. Prediction of broadband ground-motion time histories: hybrid low/high- frequency method with correlated random source parameters. Bull Seismol Soc Am 2006;96:2118–30.
[26] Mobarakeh AA, Rofooei FR, Ahmadi G. Simulation of earthquake records using time-varying Arma (2,1) model. Probab Eng Mech 2002;17:15–34.
[27] Rofooei FR, Mobarake A, Ahmadi G. Generation of artificial earthquake records with a nonstationary Kanai–Tajimi model. Eng Struct 2001;23:827–37.
[28] Sgobba S, Stafford PJ, Marano GC, Guaragnella C. An evolutionary stochastic ground-motion model defined by a seismological scenario and local site conditions. Soil Dyn Earthq Eng 2011;31:1465–79.
[29] Graves RW, Pitarka A. Broadband ground-motion simulation using a hybrid approach. Bull Seismol Soc Am 2010;100:2095–123.
[30] Boore DM. Stochastic simulation of high-frequency ground motions based on seismological models of the radiated spectra. Bull Seismol Soc Am 1983;73:1865–94.
[31] Baptie B. Seismogenesis and state of stress in the UK. Tectonophysics 2010;482:150–9.
[32] Musson RMW. The seismicity of the British Isles. Ann Geophys 1996;39.
[33] Ambraseys NN, Smit PM, Douglas J, Margaris B, Sigjornsson R, Olafsson S, Suhadolc P, Costa G. Internet site for European strong-motion data. Boll Geofis Teor Ed Appl 2004;45:113–29.
[34] Bommer JJ, Papaspiliou M, Price W. Earthquake response spectra for seismic design of nuclear power plants in the UK. Nucl Eng Des 2011;241:968–77.
[35] Musson RMW. Design earthquakes in the UK. Bull Earthq Eng 2004;2:101–12.
[36] Johnston AC, Coppersmith KJ, Kanter LR, Cornell CA. The earthquakes of stable continental regions, in: TR-102261. Palo Alto, California, USA: Electric Power Research Institute; 1994.
[37] Rietbrock A, Strasser F, Edwards B, Stochastic A. Earthquake ground-motion prediction model for the United Kingdom. Bull Seismol Soc Am 2013;103:57–77.
[38] Musson RMW. The case for large $M > 7$ earthquakes felt in the UK in historical times. In: Fréchet J, Meghraoui M, Stucchi M, editors. Historical seismology. Netherlands: Springer; 2008. p. 187–207.
[39] Baptie B, Ottemoller L, Sargeant S, Ford G, O'Mongain A. The Dudley earthquake of 2002: a moderate sized earthquake in the UK. Tectonophysics 2005;401:1–22.
[40] Ottemöller L, Baptie B, Smith NJP. Source parameters for the 28 April 2007 *Mw* 4.0 earthquake in Folkestone, United Kingdom. Bull Seismol Soc Am 2009;99:1853–67.

[41] Ottemöller L, Sargeant S. Ground-motion difference between two moderate-size intraplate earthquakes in the United Kingdom. Bull Seismol Soc Am 2010;100:1823–9.
[42] Musson RMW, Sargeant S. Eurocode 8 seismic hazard zoning maps for the UK. Technical Report, CR/07/125N. Keyworth, Nottingham, UK: British Geological Survey; 2007.
[43] Goes S, Loohuis JJP, Wortel MJR, Govers R. The effect of plate stresses and shallow mantle temperatures on tectonics of northwestern Europe. Glob Planet Chang 2000;27:23–38.
[44] Ambraseys NN. Intensity-attenuation and magnitude-intensity relationships for northwest european earthquakes. Earthq Eng Struct Dyn 1985;13:733–78.
[45] Young JB, Presgrave BW, Aichele H, Wiens DA, Flinn EA. The Flinn–Engdahl regionalisation scheme: the 1995 revision. Phys Earth Planet Inter, 96; 1996. p. 223–97.
[46] Akkar S, Sandıkkaya MA, Şenyurt M, Azari Sisi A, Ay BÖ, Traversa P, Douglas J, Cotton F, Luzi L, Hernandez B, Godey S. Reference database for seismic ground-motion in Europe (RESORCE). Bull Earthq Eng 2014;12:311–39.
[47] Douglas J. Ground-motion prediction equations 1964–2010. Final Report BRGM/RP-59356-FR. Orléans, France: BRGM; 2011.
[48] Ambraseys NN, Free MW. Surface-wave magnitude calibration for European Region Earthquakes. J Earthq Eng 1997;1:1–22.
[49] Johnston AC. Seismic moment assessment of earthquakes in stable continental regions—I. Instrumental seismicity. Geophys J Int 1996;124:381–414.
[50] Ambraseys NN, Douglas J, Sarma SK, Smit PM. Equations for the estimation of strong ground motions from Shallow Crustal Earthquakes using data from europe and the middle east: horizontal peak ground acceleration and spectral acceleration. Bull Earthq Eng 2005;3:1–53.
[51] Abrahamson N, Shedlock KM. Overview. Seismol Res Lett 1997;68:9–23.
[52] Musson RMW. British earthquakes. Proc Geol' Assoc 2007;118:305–37.
[53] Mavroeidis GP, Papageorgiou AS. A mathematical representation of near-fault ground motions. Bull Seismol Soc Am 2003;93:1099–131.
[54] Goda K, Aspinall W, Taylor CA. Seismic hazard analysis for the U.K.: sensitivity to spatial seismicity modelling and ground motion prediction equations. Seismol Res Lett 2013;84:112–29.
[55] Gregor N, Abrahamson NA, Atkinson GM, Boore DM, Bozorgnia Y, Campbell KW, Chiou BSJ, Idriss IM, Kamai R, Seyhan E, Silva W, Stewart JP, Youngs R. Comparison of NGA-West2 GMPEs. Earthq Spectra 2014;30:1179–97.
[56] Akkar S, Bommer JJ. Empirical equations for the prediction of PGA, PGV, and spectral accelerations in Europe, the Mediterranean Region, and the Middle East. Seismol Res Lett 2010;81:195–206.
[57] Douglas J, Akkar S, Ameri G, Bard P-Y, Bindi D, Bommer J, Bora S, Cotton F, Derras B, Hermkes M, Kuehn N, Luzi L, Massa M, Pacor F, Riggelsen C, Sandıkkaya MA, Scherbaum F, Stafford P, Traversa P. Comparisons among the five ground-motion models developed using RESORCE for the prediction of response spectral accelerations due to earthquakes in Europe and the Middle East. Bull Earthq Eng 2014;12:341–58.
[58] Boore DM, Joyner WB, Fumal TE. Estimation of response spectra and peak accelerations from Western North American Earthquakes: an interim report. Menlo Park, California, USA: USGS; 1993.
[59] Douglas J, Halldórsson B. On the use of aftershocks when deriving ground-motion prediction equations. In: Proceedings of the 9th U.S. national and 10th Canadian conference on earthquake engineering. Toronto, Ontario (Canada); 2010.
[60] Papadimitriou K. Stochastic characterization of strong ground motion and applications to structural response. In: Pasadena, California: Earthquake Engineering Research Laboratory, California Institute of Technology; 1990.
[61] Liao S, Zerva A. Physically compliant, conditionally simulated spatially variable seismic ground motions for performance-based design. Earthq Eng Struct Dyn 2006;35:891–919.
[62] Brune JN. Tectonic stress and the spectra of seismic shear waves from earthquakes. J Geophys Res 1970;75:4997–5009.
[63] Arias A. A measure of earthquake intensity. In: Hansen RJ, editor. Seismic design for nuclear power plants. Cambridge, Massachusetts, USA and London, UK: MIT Press; 1970.
[64] Penzien J, Watabe M. Characteristics of 3-dimensional earthquake ground motions. Earthq Eng Struct Dyn 1975;3:365–73.
[65] Kubo T, Penzien J. Time and frequency domain analyses of three dimensional ground motions San Fernando Earthquake. Berkeley, California, USA: Earthquake Engineering Research Center; 1976.
[66] Rawlings JO, Pantula SG, Dickey DA. Applied regression analysis: a research tool. Springer; 1998.
[67] Abrahamson N, Youngs R. A stable algorithm for regression analyses using the random effects model. Bull Seismol Soc Am 1992;82:505–10.
[68] PML. British earthquakes, Technical Report 115/82, Principia Mechanica Ltd., London; 1982.
[69] PML. Seismological studies for UK hazard analysis, Technical Report 346/85, Principia Mechanica Ltd., London; 1985.
[70] Musson RMW, Marrow PC, Winter PW. Attenuation of earthquake ground motion in the UK. Report AEA/CS/16422000/ZJ745/004. AEA Technology Consultancy Services; 1994. p. 30.
[71] Bommer JJ, Stafford PJ, Alarcón JE, Akkar S. The Influence of magnitude range on empirical ground-motion prediction. Bull Seismol Soc Am 2007;97:2152–70.
[72] Akkar S, Sandıkkaya MA, Bommer JJ. Empirical ground-motion models for point- and extended-source crustal earthquake scenarios in Europe and the Middle East. Bull Earthq Eng 2014;12:359–87.
[73] Dahle A, Bungum H, Kvamme LB. Attenuation models inferred from intraplate earthquake recordings. Earthq Eng Struct Dyn 1990;19:1125–41.
[74] Toro GR, Abrahamson NA, Schneider JF. Model of strong ground motions from earthquakes in Central and Eastern North America: best estimates and uncertainties. Seismol Res Lett 1997;68:41–57.
[75] Campbell KW. Prediction of strong ground motion using the hybrid empirical method and its use in the development of ground-motion (attenuation) relations in Eastern North America. Bull Seismol Soc Am 2003;93:1012–33.
[76] Liang JZ, Hao H, Gaull BA, Sinadinovski C. Estimation of strong ground motions in Southwest Western Australia with a combined green's function and stochastic approach. J Earthq Eng 2008;12:382–405.
[77] Kennedy J, Hao H, Gaull B. Earthquake ground motion attenuation relations for SWWA. New South Wales, Australia: Earthquake Engineering in Australia; 2005 pp. Paper 15.
[78] Raghu Kanth STG, Iyengar RN. Estimation of seismic spectral acceleration in Peninsular India. J Earth Syst Sci 2007;116:199–214.
[79] Chen L. Ground motion attenuation relationships based on Chinese and Japanese strong ground motion data. Pavia, Italy: European School for Advanced Studies in Reduction of Seismic Risk, ROSE School; 2008.
[80] Boore DM, Joyner WB. Site amplifications for generic rock sites. Bull Seismol Soc Am 1997;87:327–41.
[81] Cotton F, Scherbaum F, Bommer J, Bungum H. Criteria for selecting and adjusting ground-motion models for specific target regions: application to central europe and rock sites. J Seismol 2006;10:137–56.
[82] Van Houtte C, Drouet S, Cotton F. Analysis of the origins of κ (Kappa) to compute hard rock to rock adjustment factors for GMPEs. Bull Seismol Soc Am 2011;101:2926–41.
[83] Beyer K, Bommer JJ. Relationships between median values and between aleatory variabilities for different definitions of the horizontal component of motion. Bull Seismol Soc Am 2006;96:1512–22.
[84] Bakun WH, McGarr A. Differences in attenuation among the stable continental regions. Geophys Res Lett 2002;29:2121.